Pre-attentive Pitch Processing of Harmonic Complex Sounds at Sensor and Source Levels: Comparing Simultaneously Recorded EEG and MEG Data

Talya C Inbar, Jean-Michel Badier, Christian Bénar, Khoubeib Kanzari, Mireille Besson, Valérie Chanoine

Title: Pre-attentive pitch processing of harmonic complex sounds at sensor and source levels: comparing simultaneously recorded EEG and MEG data.

Authors: Talya C. Inbar[1, 2], Jean-Michel Badier[2,3], Christian Bénar[2,3], Khoubeib Kanzari[3], Mireille Besson[1,2] and Valérie Chanoine[2, 4]

Affiliations

1. Aix Marseille Univ, CNRS, CRPN, Marseille, France
2. Institute for Language and Communication in the Brain, Aix-en-Provence, France
3. Aix Marseille Univ, INSERM, INS, Inst Neurosci Syst, Marseille, France
4. Aix Marseille Univ, CNRS, LPL, Aix-en-Provence, France

Corresponding author: Valerie.Chanoine@univ-amu.fr

ORCID:

- Jean-Michel Badier: 0000-0002-7272-6455
- Christian Bénar: 0000-0002-3339-1306
- Mireille Besson: 0000-0002-9549-5274
- Valérie Chanoine: 0000-0002-3492-8160

Abstract

Electroencephalography (EEG) and magnetoencephalography (MEG), two of the most widely used tools for studying human brain dynamics, are thought to have varying spatial resolutions. Here, we simultaneously recorded EEG and MEG data from 14 participants to directly compare their sensitivities — at both the sensor and source levels — to the auditory Mismatch Negativity (MMN in EEG and MMNm in MEG) elicited by pitch deviants. At the sensor level, we observed that negative components emerged in early (100-190 ms) and late (260-420 ms) latency windows. These responses displayed a fronto-central distribution in EEG and a centro-parietal distribution in MEG. MEG also yielded larger effect sizes than EEG, likely reflecting differences in signal-to-noise ratio between MEG and EEG. At the source level, our findings support the involvement of a fronto-temporal auditory MMN network. Both EEG and MEG identified generators in the superior temporal gyrus, Heschl's gyrus, interior frontal gyrus, and insular regions. Notably, EEG source localization revealed additional generators in the left superior temporal sulcus not detected by MEG, whereas MEG identified late components generators in the right hemisphere that were not observed with EEG. Taken together, these results suggest that EEG and MEG may provide complementary perspectives on auditory processing. However, given the inherent complexity of comparing data acquired with different methodologies and the limited sample size, our conclusions should be regarded as

preliminary.

Keywords

EEG, MEG, MEEG, Mismatch Negativity (MMN), pre-attentive auditory processing, harmonic complex sounds.

Statements and Declarations

The authors declare that there is no conflict of interest.

1 Introduction

Electroencephalography (EEG) and magnetoencephalography (MEG) are two of the most ubiquitous tools used to study human brain dynamics. By recording the electrical (EEG) or magnetic (MEG) activity generated by the brain with excellent temporal resolution, both methods allow for precise tracking of time course changes in cerebral networks. EEG and MEG are thought to provide complementary spatial information, as MEG detects neural currents preferentially from tangential sources to the brain surface and EEG detects both tangential and radial sources (Puce and Hämäläinen 2017). Thus, the benefits of combining information gained from these two methods has long been of interest in the field of cognitive neuroscience (Huotilainen et al. 1998). At the same time, MEG has traditionally been considered to have better spatial resolution than EEG. With the present study, we aim to directly address this claim by comparing simultaneous EEG and MEG recordings, first at the level of the sensors (electrodes and captors) and second, at the level of the sources. To do so, we focused on the auditory Mismatch Negativity (MMN), a robust and widely studied component in cognitive neuroscience.

Since its original description as a signature of pre-attentive processing (Näätänen et al. 1978), the MMN has been widely studied in cognitive and clinical science research. In auditory contexts, it is elicited by a change in the features of sound stimuli (e.g., frequency, duration, intensity, or timbre) as compared to a standard stimulus while participants are not paying attention to the stimuli (Näätänen et al. 1978).The MMN is a difference wave; it is computed as the difference in brain responses to deviant and standard stimuli. Because it is a pre-attentive component, the MMN has held unique significance for understanding cognition in diverse contexts: in infants and young children (Gupta and Bhardwaj 2022), during sleep (Atienza et al. 2002), and in the study of pathologies (Umbricht et al. 2003; Todd et al. 2012). Its importance and high reproducibility across experiments, conditions, and modalities make the MMN (or MMNm, the MEG equivalent) a relevant measure for comparing the information captured by EEG and MEG. Here, we focus on the auditory MMN and MMNm elicited by changes in sound frequency between standard and deviant stimuli. In doing so, we aim to determine how simultaneously recorded MMN and MMNm signatures compare in terms of latency, amplitude, and scalp distribution at the sensor level, and in terms their origin at the source level.

At the sensor level, the auditory MMN is known to be distributed primarily over fronto-central regions with a peak latency of about 150-250 ms (Sams et al. 1985; Rinne et al. 2000; Näätänen et al. 2004). Similar latencies and scalp distribution have been reported for its magnetic counterpart, the MMNm (Huotilainen et al. 1998).

A later negative deflection, typically occurring between 260 and 420 ms, has also been reported in response to both complex auditory stimuli—such as syllables and words—and simpler ones like tones ((Neuhoff et al. 2012). Although often labeled as 'late MMN', this response closely matches the temporal and topographical characteristics of the N2/N2m complex. Meta-analytic reviews of late auditory event-related potentials have emphasized that negative components within this latency range are more reliably associated with the N2, particularly in paradigms involving higher-order auditory deviance detection or cognitive control mechanisms (Tomé et al. 2015).

At the source level, the identification of auditory MMN generators has been the focus of several experiments over the last decades. However, describing a clear MMN network remains challenging, in part due to the lack of uniformity of stimuli and analysis methodology across EEG and MEG source localization studies. In an early EEG dipole source localization study by Scherg et al. (1989), frequency deviant auditory stimuli were used to evoke MMN responses which were localized to the supratemporal plane of the auditory cortex — extending from anterior to posterior subregions, from the Planum Polare (PP), through Heschl’s gyrus (HG, housing the primary auditory cortex), to the Planum Temporale (PT). These regions, as well as the Sylvian fissure, were also identified in MEG studies using sinusoidal tone bursts with frequency deviant stimuli (Sams et al. 1985; Hari 1990; Huotilainen et al. 1998) and with auditory stimuli that varied in frequency, duration, and interstimulus interval (Levänen et al. 1996). In another early EEG study, scalp radial current density analysis was used to analyze MMN responses to dichotic auditory frequency stimuli, again revealing the supratemporal plane of the auditory cortex as an MMN generator, together with frontal regions (Giard et al. 1990).

More recently, an EEG study using binaural tone stimuli identified the bilateral precentral gyrus and medial frontal gyrus as major MMN generators, with maximum activity stemming from the right precentral gyrus (Takahashi et al. 2013). Further, Lecaignard et al. (2021) used auditory frequency and intensity deviant stimuli for the quantitative evaluation of EEG, MEG, and fused EEG-MEG modalities in MMN source localization. Based on EEG data, they identified MMN generators in the anterior supratemporal plane as well as in the posterior superior temporal gyrus. Meanwhile, unimodal MEG source reconstruction located generators in the posterior inferior frontal gyrus and the supratemporal plane, from Heschl’s gyrus (HG) to the Planum Polare (PP). In sum, as source localization technologies have advanced, MMN origins within and surrounding the supratemporal plane have been refined using both EEG and MEG data. However, discrepancies regarding the role of frontal regions in MMN generation remain, and in the present study, we aim to address these inconsistencies to better understand how EEG and MEG data compare for localizing the MMN frequency-auditory component.

We presented participants with harmonic complex sound (HCS) stimuli that varied in frequency in an auditory oddball protocol during simultaneous EEG and MEG recording.

These specific HCS stimuli have been shown to elicit reliable MMNs in a previous study (Frey et al. 2022) thus allowing us to formulate precise hypotheses regarding MMN latency (150-250 ms) and scalp distribution (fronto-central) for EEG data. Our first goal was to confirm these hypotheses and to compare MMN results with MMNm latency and scalp distribution to better understand how EEG and MEG capture MMN signatures at the sensor level. Our second goal was to respond to discrepancies in the literature regarding MMN source localization for EEG and MEG data, with a particular interest in MMN and MMNm activity in the frontal and supratemporal regions identified in previous studies. Through a comprehensive and equivalent analysis of EEG and MEG data, we hope to better understand how these two methods capture brain activity at the sensor level and how their source localization in our study aligns with MMN networks presented in the literature.

2 Materiels and methods

2.1 Participants

A total of 21 adults participated in this experiment, but seven participants were excluded due either to low signal-to-noise ratios in EEG or MEG data or to technical issues during the simultaneous EEG/MEG recording session. The final group was comprised of 14 participants (8 women and 6 men), between 19 and 27 years old. Inclusion criteria were the absence of neurological disorders and meeting MEG compatibility criteria, which primarily meant the absence of metal objects in the body such as piercings, prostheses, or dental fillings. Participants provided written consent to participate in the study and received monetary compensation for their participation. The study was performed in accordance with Aix-Marseille University's "Committee for the Protection of Individuals" standards (CPP 2017-A03614–49).

2.2 Stimuli

Two types of auditory stimuli were presented in separate blocks of trials: harmonic complex sounds (HCS) and syllables (SYL). Only HCS data are presented here. All HCS were equated for duration (237 ms) and intensity (60 dB) and were varied in frequency to create a standard stimulus (195 Hz) as well as large (235 Hz; 40 Hz difference),

intermediate (215 Hz; 20 Hz difference), and small (200 Hz; 5 Hz difference) deviant stimuli.

2.3 **Experimental Design**

Participants were individually tested while lying down on an MEG bed in a Faraday cage with an EEG cap (64 electrodes) on their head. Auditory stimuli were delivered binaurally through plastic tubes terminating in MEG-compatible earbuds, at a volume deemed comfortable by participants at the start of each experimental block. Stimuli were presented using Presentation software (Version 11.0, Neurobehavioral Systems, Inc., Berkeley, CA; www.neurobs.com).

This experiment was organized into pre-attentive and attentive blocks; here we focus our analyses on the MMN/MMNm elicited in the pre-attentive condition. HCS were played while participants watched a self-selected silent movie. They were instructed to focus their attention on the movie without paying attention to the auditory stimuli. A total of 1,214 stimuli were presented, with 854 repetitions of the standard stimulus (including 14 at the start of each block to establish a short-term memory trace) and 120 repetitions of each deviant stimulus (i.e., large, intermediate, and small). Stimulus presentation was organized such that at least one and at most four standard stimuli were presented in between two deviant stimuli, with no more than three deviant stimuli presented successively. The stimulus-onset-asynchrony was 600 ms and the total duration of the pre-attentive HCS condition was 12.5 minutes.

2.4 **Neurophysiological Recordings**

EEG and MEG were recorded simultaneously from 64 EEG electrodes (Ag/AgCl EEG cap, Brain Products amplifier) and 248 magnetometers (4D whole head Neuroimaging system WH3600TM) at a sampling rate of 1000 Hz for EEG and 2034.51 for MEG. Electrode impedance was kept below 10 kΩ, with most impedances below 5 kΩ. The electrooculogram (EOG) was recorded from flat-type active electrodes positioned just above and below the left eye. The electrocardiogram (ECG) was recorded from two electrodes placed on the upper left side of the chest and on the lower right abdomen, respectively. The coordinates of the EEG electrode were measured by a 3D digitizer Xensor™ referenced by three fiducial markers, the nasion, and the left and right tragus. The same points were used to define the MEG referential. Five coils were fixed on each participant's EEG cap following the standard MEG procedure. These coils, the head shape,

and the electrodes were digitized using a 3-D digitizer (Polhemus Fastrack, Polhemus Corporation, Colchester, VT), which allowed us to determine the position of the head relative to the MEG captors.

2.5 **Data Analysis**

All EEG and MEG data were analyzed and visualized in Python (Version 3.10.4) using the MNE-Python package (Gramfort et al. 2013).

2.5.1. Pre-processing of EEG and MEG Data

Simultaneously recorded EEG and MEG signals were synchronized based on stimulus triggers and combined into one file using AnyWave software (Colombet et al. 2015). EEG and MEG data were pre-processed using MNE-Python. First, EEG data were re-referenced offline to the average of all channels (excluding EOG and ECG channels). Next, EEG and MEG data were IIR filtered using a low-frequency cutoff of 0.1 Hz and a high-frequency cutoff of 30 Hz and resampled at 250 Hz. Finally, physiological artifacts were removed using a signal space projection.

2.5.2. Sensor-Level Analysis: Event-Related Potentials (ERPs) and Fields (ERFs)

Pre-processed and combined EEG and MEG files were segmented into epochs beginning 100 ms before and ending 600 ms after stimulus presentation. Next, semi-automatic artifact rejection (verified visually by experimenters) was performed on each trial to exclude electrode amplitudes above 75 µV and sensor amplitudes above 5e-12 T. Baseline correction was applied in the time frame of 100 ms before stimulus onset. Activity recorded after stimulus presentation was computed relative to this baseline. The defective EEG/MEG channels were interpolated using a field interpolation technique for both EEG and MEG data (available in MNE-python tools, Gramfort et al. 2013). For each participant, epochs were time-locked and averaged relative to stimulus onset for standard stimuli and for each type of deviant stimulus (large, intermediate, and small) to extract the Event-Related Potentials (ERPs) and the Event-Related Fields (ERFs). Then, the ERP/Fs from the standard stimulus were subtracted from the ERP/Fs to each deviant stimulus to compute the difference waves, and statistical analyses were performed on these components.

Analysis of Regions of Interest (ROIs)

Grand average difference waves were calculated and plotted according to nine electrode/sensor Regions of Interest (ROIs, Figure 1) and data were averaged across four electrodes/16 sensors in each ROI. The ROIs were organized as Frontal (Left, Midline, and Right), Central (Left, Midline, and Right) and Parietal (Left, Midline, and Right).

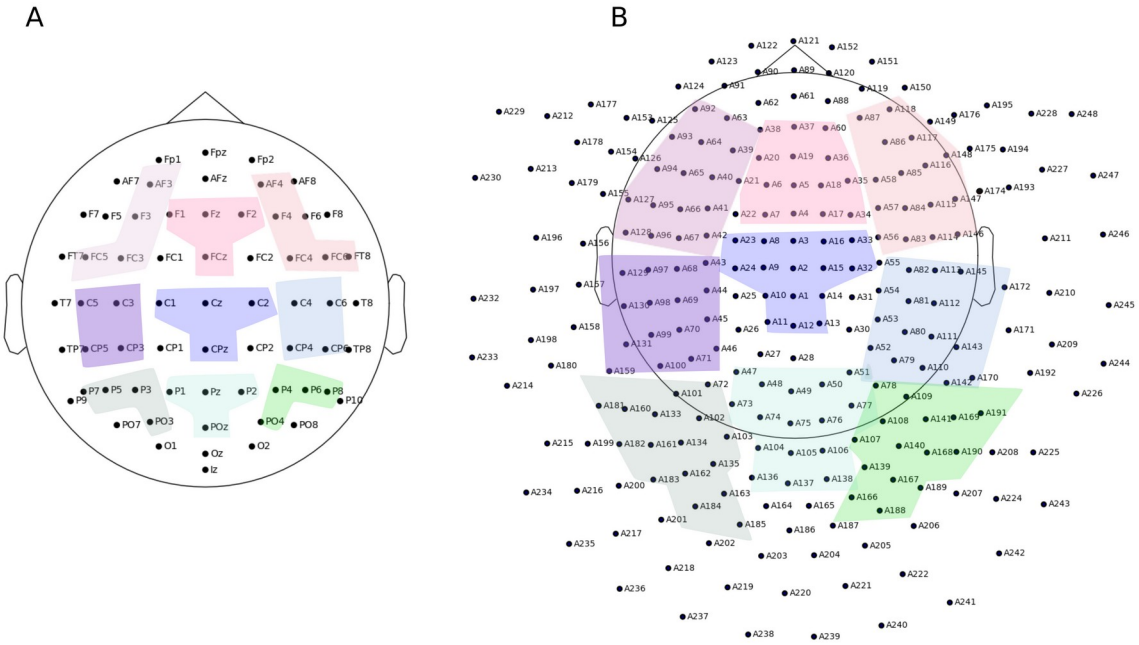

Figure 1. [Legend goes there]

Main Statistical analyses

Statistical analyses were performed using Pingouin, an open-source statistical package written in Python 3 (Vallat 2018) for Analyses of Variance (ANOVAs). Two-way repeated-measures ANOVAs were conducted to analyze the amplitude of the MMN/MMNm (the dependent variables) with deviance (3 modalities: large, intermediate and small) and ROIs (9 regions) as within-subject factors. ANOVAs were conducted in two negative component latency bands: an early band from 100 to 190 ms (components referred to as early MMN/MMNms) and a late band from 260 to 420 ms (components referred to as late MMN/MMNm/N2/N2ms, see the Discussion section for further interpretation).

In cases where the sphericity assumption was violated (Greenhouse-Geisser $\varepsilon < 0.62$), p-values were corrected using the Greenhouse-Geisser adjustment and are reported accordingly (p-GG).

To further examine the Deviance × ROI interaction, one-way repeated-measures ANOVAs with Deviance as a within-subject factor were performed separately for each component (MMN/MMNms and N2/N2ms) and for each ROI.

Post hoc pairwise comparisons between Deviance conditions were conducted using paired-sample t-tests, with p-values corrected for multiple comparisons using the Benjamini–Hochberg false discovery rate (FDR-BH; Benjamini and Hochberg 1995).

Post-hoc Power Analysis

To assess the statistical sensitivity of repeated-measures ANOVAs and paired-sample t-tests, given the relatively small sample size (N = 14 participants), post-hoc power analyses were performed (see Appendix, section 8.2, for details).

For the purposes of this study, we consider an estimated statistical power greater than 0.8 to indicate an acceptable level of sensitivity for detecting effects of interest. This threshold aligns with conventional standards in the field (Cohen 2013), while also acknowledging the inherent limitations associated with small-sample, within-subject designs.

Comparison of Early and Late Component Effect Sizes

Because EEG and MEG are recorded using different units (µV and fT, respectively), they are not directly comparable. Thus, to determine which of the two methods, EEG or MEG, is more effective in measuring our initial component of interest, the auditory MMN, we computed effect sizes as standardized measures. Based on the literature, the size of the effect was considered as small for values between 0.2 and 0.5, moderate for values between 0.5 and 0.8, and large for values above 0.8 (Cohen 2013).

We focused on the large deviant stimuli, which elicited the largest early and late negative components, for these analyses. Because the large deviant consistently elicited the strongest and most reliable responses across both EEG and MEG modalities, it was the most suitable candidate for assessing and comparing the sensitivity of the two recording methods. We chose to omit weaker deviant conditions at this stage of analysis as they could have introduced additional noise and diluted the comparison of effect sizes

between modalities. Thus, we first estimated the latency of their maximum amplitude to large deviants across all channels. As previously mentioned, for comparison purposes, and based on Global Field Power (GFP) and Root Mean Square (RMS) analyses, we considered two latency windows, one for the early negative components (100-190 ms) and one for the late negative components (260-420 ms; Figure 2). Topographical maps corresponding to these two latency windows were then generated (Figure 3). Finally, difference waves were computed for each participant and for each sensor (large deviant stimuli minus standard stimuli) and the mean MMN/MMNm/N2/N2m amplitudes were extracted for each latency band.

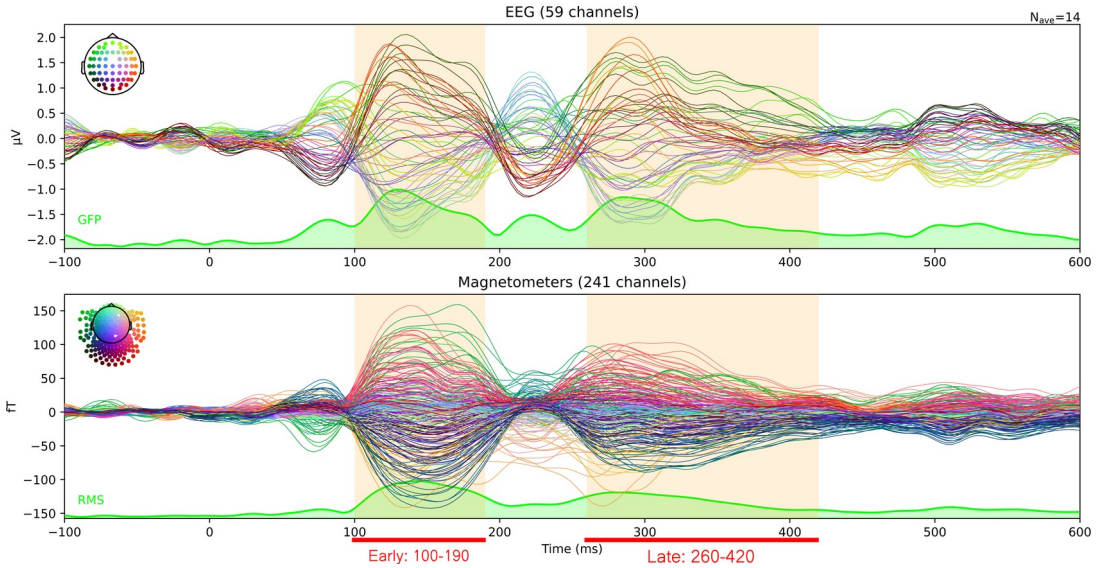

Figure 2. [Legend goes there]

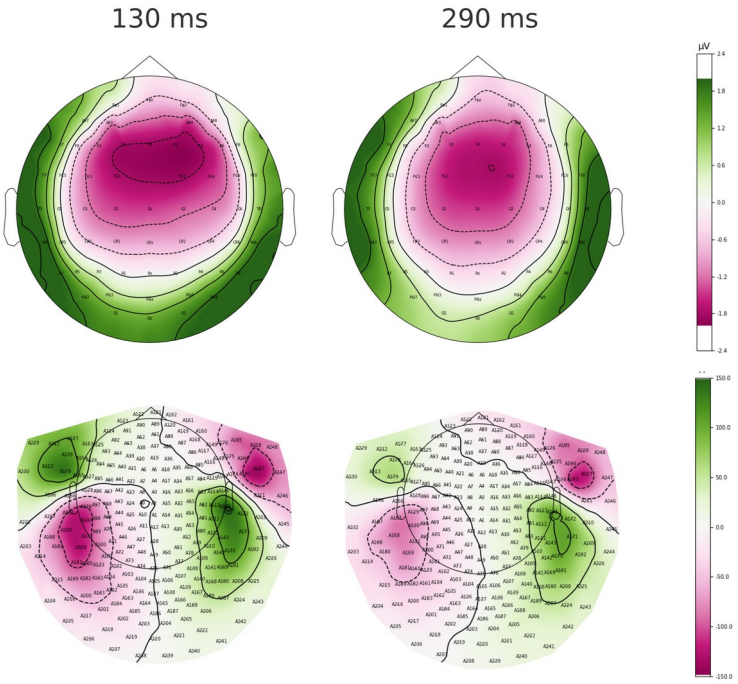

Figure 3. [Legend goes there]

One-way repeated-measures ANOVAs were performed for each participant, sensor, and latency window, with deviance as the within-subject factor. These analyses tested whether the MMN/MMNm/N2/N2m amplitudes evoked by large deviant stimuli differed significantly from a null (zero) baseline. The dependent variable was the MMN/MMNm/N2/N2m amplitude, and the resulting effect sizes (specifically, the square root of the partial eta squared, referred as R) were computed. P-values were adjusted for multiple comparisons using a Bonferroni correction.

In sum, for each participant and each sensor showing a statistically significant difference between the MMN/MMNm/N2/N2m amplitudes in response to large deviant stimuli and zero amplitude, we compared the effect sizes obtained in EEG and MEG, in their respective time windows.

2.5.3. Source-Level Analysis

Source Estimation

To estimate the neural sources underlying the recorded signal, we performed source

reconstruction on combined EEG and MEG data in MNE-python (Gramfort et al. 2013). For the inverse solution, we first computed the forward model separately for EEG and MEG. The forward model — also known as the gain or leadfield matrix — maps neural source activity to the expected measurements at the sensors. It requires three key components: a head (volume conductor) model, a source space (a set of dipole locations), and the relative positions of the sensors.

Before computing the forward model, spatial coregistration must be performed to align the MEG sensor positions, digitized scalp landmarks, and MRI anatomy. In our case, this was done using a standardized MRI template (Reuter et al. 2012) individually aligned to each subject's digitization. This alignment process was conducted using the automated co-registration method provided in MNE-python (Houck and Claus 2020) with visual inspection for quality control.

The head model, necessary for understanding how current flows from brain sources to EEG and MEG sensors on or above the scalp, depends on both head geometry and tissue conductivity. For our head model, Boundary Element Model (BEM) surfaces were created using the FreeSurfer watershed algorithm (Ségonne et al. 2004) as implemented in MNE-python. To ensure consistency between EEG and MEG models, the same three tissue layers were considered: inner skull, outer skull, and scalp surfaces. The default electrical conductivities used in MNE-python were 0.3 Siemens per meter (S/m) for the brain and the scalp, and 0.006 S/m for the skull.

The cortical source space was generated by recursively subdividing the faces of an octahedron four times (oct4) in both hemispheres. To reduce computational load while maintaining broad cortical coverage, we downsampled the source space to 516 vertices, evenly distributed across the cortical surface. Dipole orientation was left unconstrained to allow for more accurate alignment with true source orientations.

The forward operator was computed with a minimum distance of five millimeters from the inner skull surface to the sources. Before forward computation, EEG channels were re-referenced to the average of all EEG electrodes. Noise covariance was estimated from the pre-stimulus baseline of trials from all four experimental conditions (standard, and small, intermediate, and large deviants), using the "empirical" method provided by MNE-python.

For inverse modeling, we applied the dynamic Statistical Parametric Mapping (dSPM) algorithm (Dale et al. 2000) to the difference waves from each condition (e.g., "Large Deviant minus Standard"). A free-orientation dSPM solution was computed using MNE-python defaults: loose orientation = 1.0, depth weighting = 0.8 (Lin et al. 2006), and SNR = 3.

To obtain an overall view of the group-level dSPM maps, we performed spatial morphing of the individual dSPM data to align them across subjects (see MNE documentation for details). The morphed data were then averaged and projected onto the *fsaverage*

standard cortical surface. An illustration of this projection is shown for the “Large Deviant minus Standard” contrast at 130 ms and 190 ms post-stimulus (see Figure A1 in the Appendix).

Analysis of Regions of Interest (ROIs)

Anatomically defined parcellations are applied post hoc to summarize source estimates obtained from a distributed, anatomically unconstrained source inversion. This approach is supported by numerous studies (e.g., (Glasser et al. 2016; Schoffelen et al. 2017; Tait et al. 2021; Areces-Gonzalez et al. 2024). In other words, brain activity was first estimated at the source level without being limited to predefined regions, and this activity was subsequently grouped according to well-defined anatomical regions.

To carry out this method, we first defined standardized parcels on a template surface (fsaverage), based on one of the Schaefer brain atlases (Schaefer et al. 2018). These atlases were generated from resting-state fMRI data of 1,489 subjects, using a gradient-weighted Markov Random Field (gwMRF) model to produce parcellations at various spatial resolutions (100, 200, 400, 600, 800, and 1,000 parcels).

For our analysis, we used the 400-parcel, 17-network version of the Schaefer atlas, as later refined by Kong et al. (2021), and selected only a subset of parcels presumed to be associated with the mismatch negativity (MMN) response. This selection was guided by a recent study in which EEG and MEG were simultaneously recorded to localize brain regions generating the auditory MMN in response to frequency-deviant stimuli (Lecaignard et al. 2021).

Table A1 lists the peak MNI coordinates of the clusters identified in that later study as MMN generators within the 150–200 ms time window (courtesy of Françoise Lecaignard). The corresponding Schaefer parcel names, as used in the present study, are also listed for reference (see Table A1 and section 8.2. in the Appendix for further details).

Based on the Schaefer atlas and in line with the findings of Lecaignard et al. (2021), we extracted eighteen broad regions of interest (ROIs), distributed bilaterally across both cerebral hemispheres. Figure 4 illustrates the projection of these ROIs onto the left and right hemispheres. A visual region, located in the occipital lobe, served as a control.

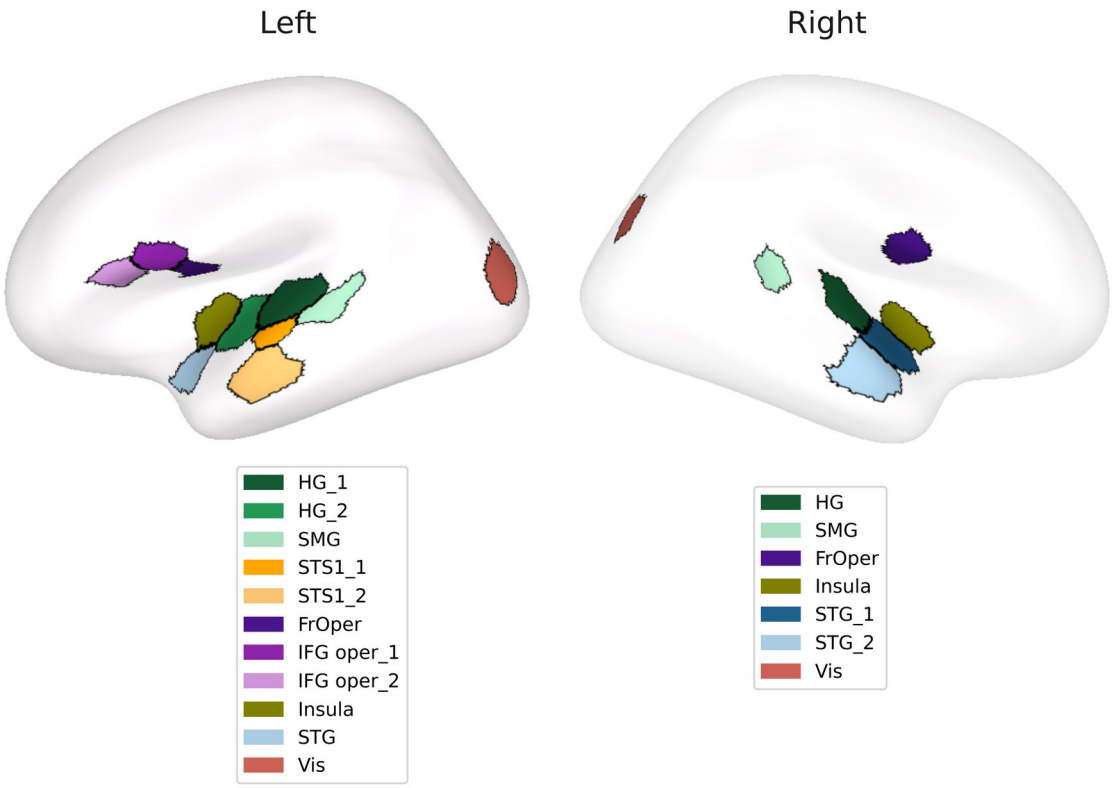

Figure 4. [Legend goes there]

The Source Time Courses (STC) were summarized at vertices using singular value decomposition within each ROI. Only the first singular vector was retained as the representative ROI STC, as it closely reflected the amplitude and phase of the average signal within the ROI (see the MNE function ‘extract_label_time_course’ with the ‘pca_flip’ option).

The extraction of source time courses (STCs) failed for one of the ROIs — the right insula — due to the absence of any vertex within this region in the 516-vertex source space used in this study. Consequently, the right insula ROI was excluded from all subsequent analyses. The spatial correspondence between the defined ROIs and the distributed source model is detailed in Appendix, Section 8.2.3.

To evaluate MMN/MMnm/N2/N2m amplitudes at the source level, the absolute value of the first singular vector was used in the statistical analyses. As in the sensor-level analyses, repeated-measures ANOVAs were conducted with deviance (three levels: large, intermediate, and small) and ROI (17 regions, excluding the right insula) as within-subject factors. These analyses were performed separately for two latency windows corresponding to the early MMN/MMNm response (100–190 ms) and the late MMN/MMNm/N2/N2m response (260–420 ms).

3 Results

3.1 Sensor Level Analysis

3.1.1. EEG

Effects of Deviance and Sensor-Level Region on Early MMN Amplitudes (100 to 190 ms)

During the early MMN time window (100–190 ms), a two-way repeated-measures ANOVA revealed a significant main effect of Deviance ($F(2, 26) = 8.87$, $p < .002$, $\varepsilon = 0.79$) as well as a significant Deviance × ROI interaction ($F(16, 208) = 7.14$, p-GG $< .006$, $\varepsilon = 0.11$). The main effect of ROI ($F(8, 104) = 3.88$, p-GG $= .055$, $\varepsilon = 0.17$) did not reach conventional significance but showed a weak trend, suggesting regional variability in the overall response.

Given the relatively small sample size (N = 14), a post-hoc power analysis was conducted to evaluate the sensitivity of the statistical tests. The post-hoc power analysis revealed excellent power to detect the main effect of Deviance (1.000) and the Deviance × ROI interaction (1.000), as well as high power for the main effect of ROI (0.893). These results indicate that the study was sufficiently powered to detect medium to large effects within the repeated-measures ANOVA framework.

To further investigate the deviance × ROI interaction, separate one-way repeated-measures ANOVAs with deviance (large, intermediate, small) as the within-subject factor were conducted for each ROI.

Results revealed a consistent pattern over fronto-central sites, with large deviant stimuli eliciting significantly greater MMN amplitudes compared to both intermediate and small deviants (see Figure 5). Below, we detail the four regions that exhibit this pattern:

- **Frontal Left** (Significant effect of Deviance :$F(2, 26) = 9.00$, $p < .002$, $\varepsilon = 0.95$): Post-hoc comparisons (paired t-tests, FDR-corrected) revealed that large deviants elicited significantly greater MMN amplitudes than both small deviants ($t(13) = 3.43$, p-$fdr < .007$) and intermediate deviants ($t(13) = 3.54$, p-$fdr < .007$).
- **Frontal Midline** (Significant effect of Deviance : $F(2, 26) = 8.34$, $p < .002$, $\varepsilon = 0.73$): Post-hoc comparisons revealed that large deviants elicited significantly

greater MMN amplitudes than both small deviants ($t(13) = 3.40$, $p\text{-}fdr < .02$) and intermediate deviants ($t(13) = 2.74$, p-fdr $< .03$).

- **Frontal Right** (Significant effect of Deviance : $F(2, 26) = 7.53$, $p < .003$, $\varepsilon = 0.98$): Post-hoc comparisons revealed that large deviants elicited significantly greater MMN amplitudes than both small deviants ($t(13) = 3.69$, $p\text{-}fdr < .009$) and intermediate deviants ($t(13) = 2.77$, p-fdr $< .03$).
- **Central Midline** (Significant effect of Deviance : $F(2, 26) = 10.08$, $p < .0006$, $\varepsilon = 0.77$): Post-hoc comparisons revealed that large deviants elicited significantly greater MMN amplitudes than both small deviants ($t(13) = 3.83$, $p\text{-}fdr < .007$) and intermediate deviants ($t(13) = 3.13$, p-fdr $< .02$).

To assess the robustness of the MMN-related EEG findings, a post-hoc power analysis was conducted on one-way ANOVAs and paired t-tests (see Table A2).

In all post-hoc power analyses, MMN effects were deemed reliable in a given region only when the Deviance effect showed statistical power > 0.80 for both ANOVA and paired t-tests in at least one contrast (Large vs. Small or Large vs. Intermediate).

As shown in Table A2, the MMN-related EEG effects exhibited sufficient statistical power at the following fronto-central sites: Frontal Left, Frontal Midline, Frontal Right, and Central Midline.

These results support the reliability of the observed effects, indicating that MMN amplitude at fronto-central ROIs consistently increases with deviance magnitude, particularly when comparing large to small deviants.

Effects of Deviance and Sensor-Level Region on Late MMN/N2 Amplitudes (260 to 420 ms)

During the late time window (260–420 ms), the main effect of Deviance was significant ($F(2, 26) = 3.42$, $p < .05$, $\varepsilon = 0.68$), while the Deviance × ROI interaction showed a marginal trend ($F(16, 208) = 2.89$, p-GG $= .07$, $\varepsilon = 0.12$). The main effect of ROI also exhibited a non-significant trend ($F(8, 104) = 2.89$, p-GG $= .08$, $\varepsilon = 0.22$).

Post-hoc power analysis revealed adequate sensitivity for all effects of interest: Power for the main effect of Deviance was 0.94, indicating a high probability of detecting a true effect given the sample size (N = 14). The power for the main effect of ROI was slightly lower but still acceptable (0.86), while the power for the Deviance × ROI interaction reached 0.96, suggesting that the analysis was sufficiently powered to detect interaction effects.

To further explore the MMN/N2-related EEG responses across different ROIs, separate one-

way repeated-measures ANOVAs were performed with Deviance as a within-subject factor.

The results revealed a consistent pattern over fronto-central sites: large deviant stimuli elicited significantly greater MMN/N2 amplitudes compared to intermediate or small deviants (see Figure 5). Below, we detail the two regions exhibiting this effect:

- **Frontal Midline** (Significant effect of Deviance: $F(2, 26) = 4.04$, $p < .03$, $\varepsilon = 0.78$): Post-hoc comparisons revealed a trend toward greater MMN/N2 amplitudes for large deviants compared to both small ($t(13) = 2.25$, p-fdr = .06) and intermediate deviants ($t(13) = 2.74$, p-fdr = .06).
- **Central Midline** (Significant effect of Deviance: $F(2, 26) = 4.55$, $p < .02$, $\varepsilon = 0.81$): Large deviants elicited significantly greater MMN/N2 amplitudes than small deviants ($t(13) = 3.14$, p-fdr < .03), with a marginal trend observed for the comparison with intermediate deviants ($t(13) = 2.17$, p-fdr = .07).

As shown in Table A3, the MMN/N2-related effect can be considered statistically reliable within the Central Midline region, where statistical power exceeded 0.8 for both the ANOVA and the paired t-test in the Large vs. Small contrast. In contrast, although the Frontal Midline region showed sufficient power for the ANOVA, none of the paired t-test comparisons reached the 0.8 threshold, and thus this region does not meet the reliability criterion.

Overall, these results indicate that at fronto-central regions of interest for the early MMN, and at the central midline site for the late MMN/N2, response amplitudes systematically increase with deviance magnitude—large deviants eliciting significantly stronger responses than intermediate or small ones. These findings underscore the sensitivity of the fronto-central early MMN and central midline late MMN/N2 responses to salient auditory changes, particularly in the case of large deviations from the standard stimuli.

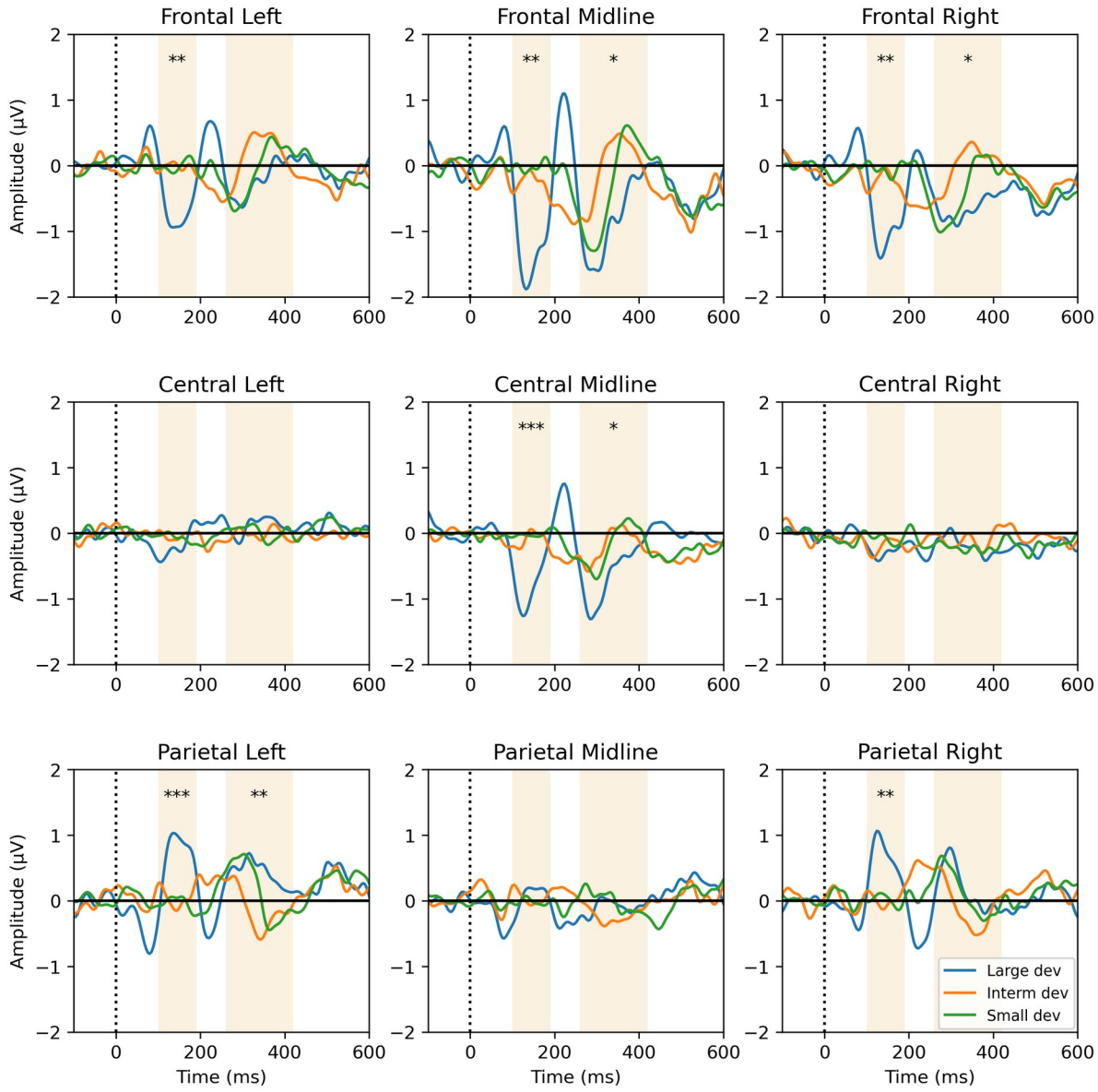

Figure 5. [Legend goes there]

3.1.2. MEG

Effects of Deviance and Sensor-Level Region on Early MMNm Amplitudes (100 to 190 ms)

During the MMNm time window (100–190 ms), the main effect of Deviance was not significant ($F(2, 26) = 0.74$, $p = 0.48$, $\varepsilon = 0.96$), indicating that, when averaged across sensor regions, MMNm amplitudes did not differ reliably across the three deviance levels. In contrast, both the main effect of ROI and the Deviance × ROI interaction reached high

significance (ROI: $F(8, 104) = 12.38$, p-GG $< .0002$, $\varepsilon = 0.24$; interaction: $F(16, 208) = 12.61$, p-GG $< .0005$, $\varepsilon = 0.10$), suggesting that MMNm amplitudes varied by region in a deviance-dependent manner.

Power analyses further indicated that the test had low sensitivity to detect the Deviance effect (Power $= 0.43$), whereas it had excellent sensitivity for both the ROI effect and the Deviance × ROI interaction (Power > 0.95 for both).

To further examine the interaction, separate one-way repeated-measures ANOVAs with deviance as a factor were conducted for each ROI. The results revealed that at left and right centro-parietal sites (but not over the midline), large deviant stimuli consistently evoked larger MMNm amplitudes than intermediate and small deviants (see Figure 6).

Below, we detail the four regions exhibiting this effect:

- **Central Left** (Significant effect of Deviance: $F(2, 26) = 12.71$, $p < .0002$, $\varepsilon = 0.61$): Large deviants elicited significantly greater MMNm amplitudes than both small ($t(13) = 4.19$, p-fdr $< .001$) and intermediate deviants ($t(13) = 3.32$ p-fdr $< .006$).
- **Central Right** (Effect of Deviance: $F(2, 26) = 2.55$, $p = .09$, $\varepsilon = 0.66$): Large deviants elicited significantly greater MMNm amplitudes than both small ($t(13) = 4.09$, p-fdr $< .002$) and intermediate deviants ($t(13) = 3.29$ p-fdr $< .006$).
- **Parietal Left** (Significant effect of Deviance: $F(2, 26) = 17.10$, $p < .0001$, $\varepsilon = 0.70$): Large deviants elicited significantly greater MMNm amplitudes than both small ($t(13) = 4.62$, p-fdr $< .002$) and intermediate deviants ($t(13) = 4.29$, p-fdr $< .002$).
- **Parietal Right** (Significant effect of Deviance: $F(2, 26) = 23.17$, $p < .0001$, $\varepsilon = 0.83$): Large deviants elicited significantly greater MMNm amplitudes than both small ($t(13) = 5.59$, p-fdr $< .0003$) and intermediate deviants ($t(13) = 4.78$, p-fdr $< .0006$).

Overall, the results revealed MMNm-related MEG effects at both left and right centro-parietal sites. The post-hoc power analysis (Table A4) confirmed the statistical reliability of these effects.

Effects of Deviance and Sensor-Level Region on Late MMNm/N2m Amplitudes (260 to 420 ms)

For the late MMNm/N2m (260–420 ms), the main effect of Deviance was not significant ($F(2, 26) = 0.77$, $p = 0.47$, $\varepsilon = 0.76$), indicating no overall amplitude differences across deviance levels when averaged over sensor regions. In contrast, the main effect of ROI ($F(8,104) = 8.13$, p-GG $< .0009$, $\varepsilon = 0.30$) and the Deviance × ROI interaction reached statistical significance ($F(16, 208) = 4.03$, p-GG $< .03$, $\varepsilon = 0.13$), suggesting a topographically specific modulation of the late MMNm/N2m response as a function of deviance level in this late latency window.

Post-hoc power analyses further supported these findings. The statistical power to detect the main effect of Deviance was low (Power = 0.39), indicating a limited sensitivity to identify potential differences across deviance levels at the global level. In contrast, the analyses revealed high power for both the main effect of ROI (Power > 0.99) and the Deviance × ROI interaction (Power > 0.99), confirming the robustness of the observed topographically specific modulation of the late MMNm/N2m response.

To further examine the interaction, separate one-way repeated-measures ANOVAs were conducted for each region of interest (ROI), with deviance as the within-subject factor. The results revealed that in the left and right centro-parietal regions (with the exception of the right central region), large deviant stimuli consistently elicited stronger late MMNm/N2m responses than both intermediate and small deviants (see Figure 6). The three regions showing this effect are detailed below:

- **Central Left** (Significant effect of Deviance: $F(2, 26) = 5.55$, p-fdr $< .01$, $\varepsilon = 0.59$): Large deviants evoked significantly greater late MMNm/N2m amplitudes than small deviants ($t(13) = 3.26$, p-fdr $< .02$), and a trend was observed for intermediate deviants ($t(13) = 2.33$, p-fdr $= .05$).
- **Parietal Left** (Significant effect of Deviance: $F(2, 26) = 11.97$, p-fdr $< .0002$, $\varepsilon = 0.66$): Large deviants elicited significantly greater late MMNm/N2m amplitudes than both small ($t(13) = 3.38$, p-fdr $< .008$) and intermediate deviants ($t(13) = 3.73$, p-fdr $< .008$).
- **Parietal Right** (Significant effect of Deviance: $F(2, 26) = 3.41$, p-fdr $< .05$, $\varepsilon = 0.81$): Large deviants evoked greater late MMNm/N2m amplitudes than small ($t(13) = 2.17$, p-fdr $= .14$, p uncorrected $< .05$) and intermediate deviants ($t(13) = 1.56$, p-fdr $= .19$), though these pairwise differences did not reach statistical significance.

Overall, the results revealed late MMNm/N2m components predominantly in the left centro-parietal regions, characterized by a consistent increase in response to large deviants.

As shown in Table A5, the late MMNm/N2m effect met the statistical reliability criterion in the Central Left and Parietal Left regions (with statistical power exceeding 0.8 for both the

ANOVA and the paired t-test in the Large vs. Small contrast). In contrast, the Parietal Right region did not reach the required power threshold in any of the paired t-test comparisons and thus cannot be considered statistically reliable under our criteria. As observed for the early MMNm, the late MMNm/N2m responses exhibited opposite polarities over the left and right centro-parietal areas.

In sum, the results revealed the early MMNm was localized in bilateral centro-parietal regions, with a consistent increase in amplitude in response to large deviants. For the late MMNm/N2m component, results showed a predominantly left-lateralized sensitivity to deviance magnitude in centro-parietal areas, with the strongest neural responses elicited by large auditory deviants.

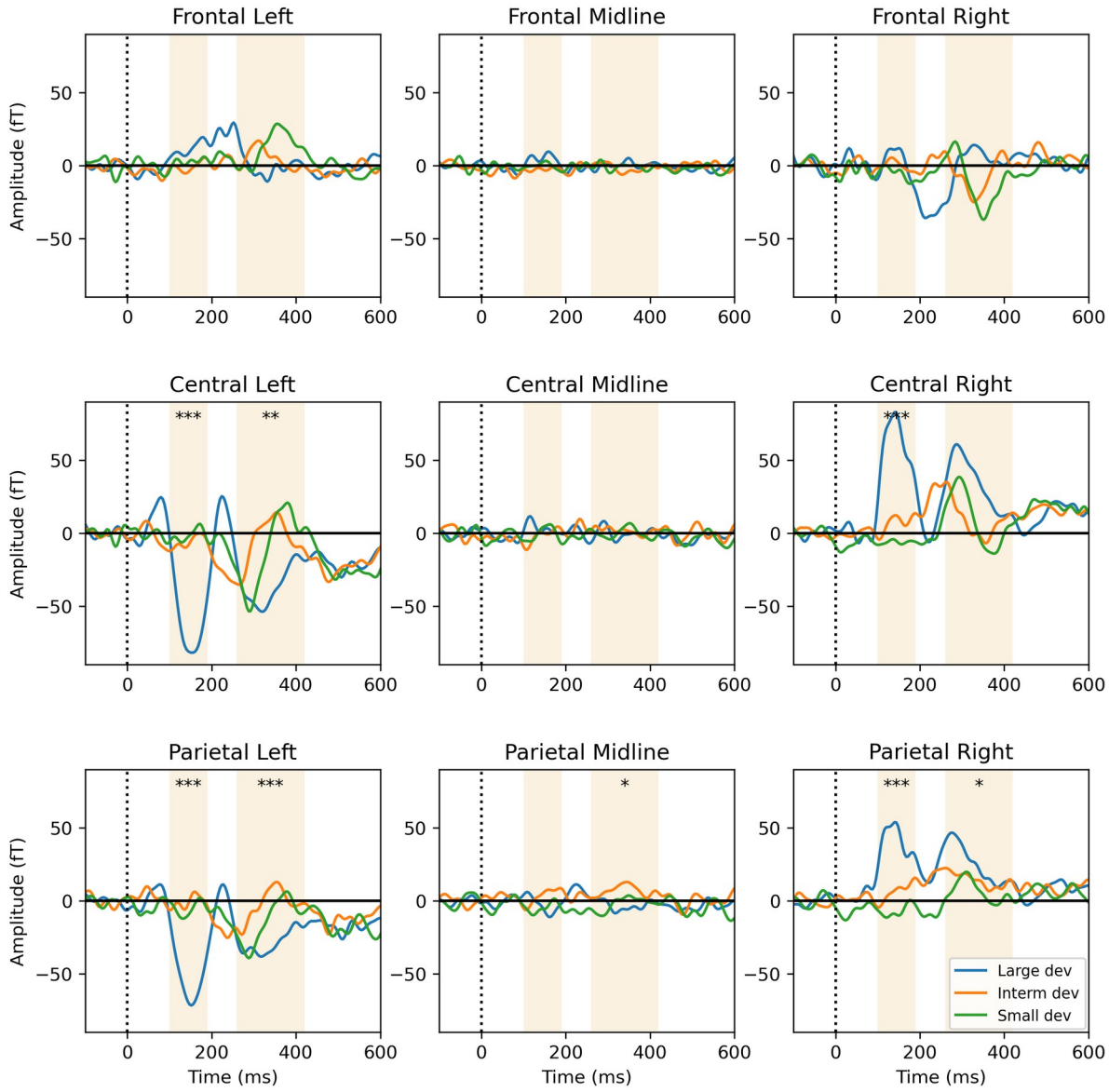

Figure 6. [Legend goes there]

3.1.3. Comparison of MMN/N2 and MMNm/N2m Effect Sizes in Early and Late Latency Windows

As a reminder, effect sizes for our negative components were derived from one-way repeated-measures ANOVAs conducted at the trial level, across participants, channels, and latency windows. These analyses assessed MMN/MMNm/N2/N2m responses, defined as the amplitude difference between responses to large deviant stimuli and standard stimuli, relative to a null baseline. Only effect sizes associated with statistically significant results are reported, based on a Bonferroni-corrected significance threshold (corrected $p < 0.05$).

For EEG, 23 out of 64 electrodes (36%) showed a significant difference for the early MMN (100-190 ms), compared to two (3%) for the late MMN/N2 (260-420 ms). For MEG, 139 out of 248 sensors (56%) showed a significant difference for the early MMNm, compared to 29 (12%) for the late MMNm/N2m. To further analyze these results, we focused on the electrodes/sensors that were significant for more than one of the 14 participants. For EEG, 12 out of 64 electrodes (19%) were significant for the MMN, and none were significant for the late MMN/N2. For MEG, 62 out of 248 sensors (25%) showed significance for the early MMNm, while 13 out of 248 sensors (5%) were significant for the late MMNm/N2m. Based on this, we selected the channels most likely to produce the largest effect sizes.

Early MMN and late MMN/N2 effect size results for the subset of significant channels are illustrated for the early and late latency windows using a boxplot representation where the effect size is represented per channel (Figures 7 and 8).

For EEG, the early MMN showed significant effect sizes at electrodes located over fronto-central and left temporal regions, with the largest median MMN effect size at electrode TP7, which corresponds to a small effect on Cohen's scale. No significant effect sizes were found for the late MMN/N2.

For MEG and for the MMNm, significant effect sizes were found for sensors located over fronto-parieto-temporal regions, bilaterally, with moderate effect sizes at eight sensors. For the late MMNm/N2m, significant effect sizes were found for sensors located over the parieto-temporal region of the right hemisphere.

In sum, the qualitative comparison of the effect size values between the EEG and MEG methods revealed that the negative component effect sizes for MEG were larger and found over a higher percentage of sensors than for EEG.

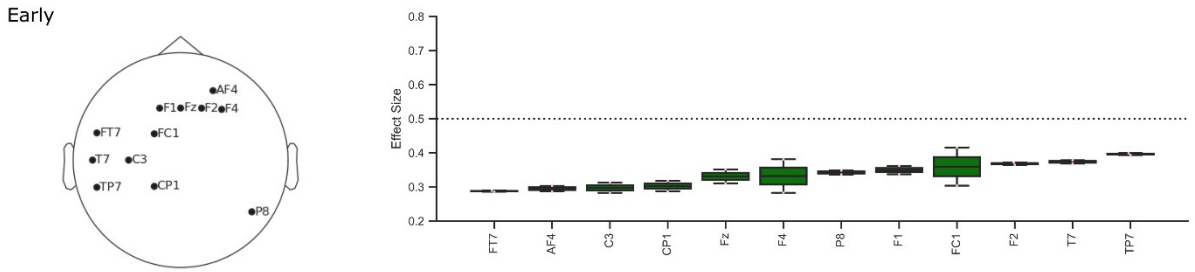

Figure 7. [Legend goes there]

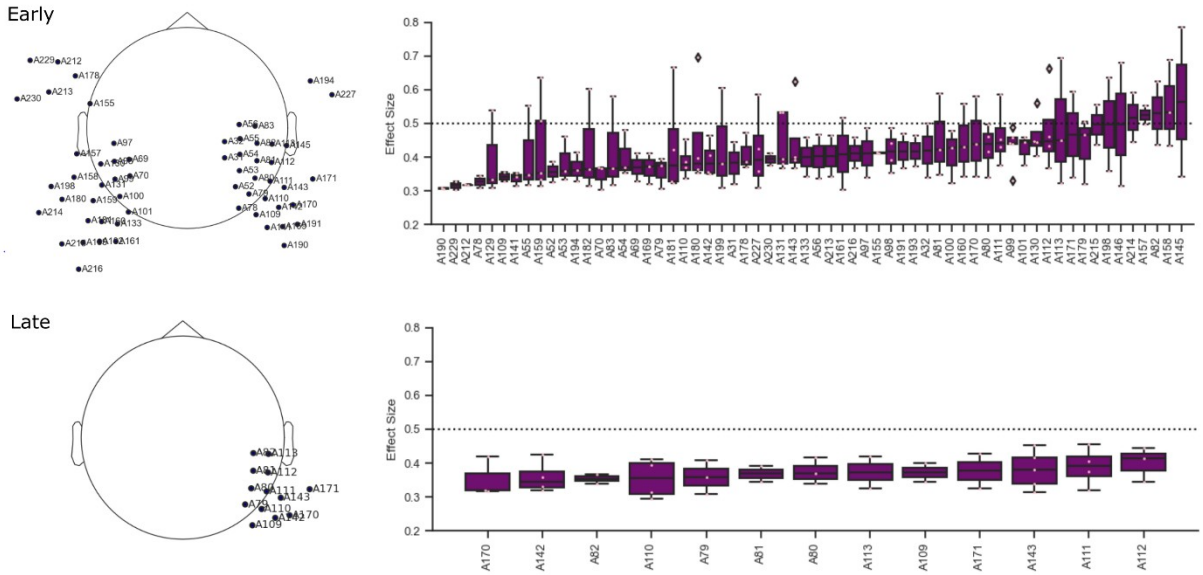

Figure 8. [Legend goes there]

3.2 **Source Level Analysis**

3.2.1. EEG

Effects of Deviance and Cortical ROI on Early MMN Amplitudes (100 to 190 ms)

For the early MMN time window, a repeated-measures ANOVA was performed with Deviance (large, intermediate, small) and cortical ROI (17 regions excluding the right insula, see Figure 4) as within-subject factors. There was a significant main effect of Deviance ($F(2, 26) = 13.70$, p-GG $< .002$, $\varepsilon = 0.56$), indicating that the neural response

significantly differed across the three stimulus conditions. The main effect of ROI was also significant ($F(16, 208) = 3.41$, p-GG $< .02$, $\varepsilon = 0.23$), reflecting variability in response magnitude across the 17 regions of interest. The Deviance × ROI interaction reached significance before correction ($F(32, 416) = 2.58$, p uncorrected $<.001$, p-GG $= .07$, $\varepsilon = 0.08$), suggesting that the effect of deviance may vary across regions.

A post-hoc power analysis was conducted due to the limited sample size ($N = 14$). The achieved power ($1 - \beta$) exceeded 0.92 for the main effects of Deviance and ROI and reached 0.84 for the Deviance × ROI interaction. These results suggest that the study was well-powered to detect main effects and the interaction.

To further examine the Deviance × ROI interaction, one-way repeated-measures ANOVAs with Deviance as a within-subject factor were performed separately for each ROI. Post-hoc pairwise comparisons between Deviance conditions were conducted using paired-sample t-tests, with p-values corrected for multiple comparisons using FDR.

Significant Deviance effects — characterized by a stronger MMN response to large compared to both small and intermediate deviant stimuli — were observed in multiple source-level regions.

- Supratemporal Planes:
    - **Left Heschl's Gyrus** (HG_1; Significant effect of Deviance: $F(2, 26) = 11.47$, p-GG $< .003$, $\varepsilon = 0.59$): Large deviants evoked significantly greater responses than small deviants ($t(13) = 3.45$, p-fdr $< .007$) and intermediate deviants ($t(13) = 3.52$, p-fdr $< .007$).
    - **Left Heschl's Gyrus** (HG_2; Significant effect of Deviance: $F(2, 26) = 12.10$, $p < .0002$, $\varepsilon = 0.67$): Large deviants evoked significantly greater responses than small deviants ($t(13) = 3.60$, p-fdr $< .005$) and intermediate deviants ($t(13) = 3.73$, p-fdr $< .005$).
    - **Right Heschl's Gyrus** (HG; Significant effect of Deviance: $F(2, 26) = 11.69$, $p < .0003$, $\varepsilon = 0.69$): Large deviants evoked significantly greater responses than small deviants ($t(13) = 3.26$, p-fdr $< .01$) and intermediate deviants ($t(13) = 4.00$, p-fdr $< .005$)
- Supramarginal Gyri:
    - **Left SMG** (Significant effect of Deviance: $F(2, 26) = 9.07$, $p < .002$, $\varepsilon = 0.62$): Large deviants evoked significantly greater responses than small deviants ($t(13) = 3.43$, p-fdr $< .02$) and intermediate deviants ($t(13) = 2.73$ p-fdr $< .03$).
    - **Right SMG** (Significant effect of Deviance: $F(2, 26) = 7.21$, $p < .002$, $\varepsilon = 0.59$): Large deviants evoked significantly greater responses than small deviants ($t(13) = 2.83$, p-fdr $< .03$) and intermediate deviants ($t(13) =$

2.65, p-fdr < .03).

- Superior Temporal Sulci (Left Hemisphere):
    - **Left STS1_1** (Significant effect of Deviance: F(2, 26) = 7.44, p < .003, ε = 0.62): Large deviants evoked significantly greater responses than small deviants (t(13) = 2.78, p-fdr < .03) and intermediate deviants (t(13) = 2.91, p-fdr < .03).
    - **Left STS1_2** (Significant effect of Deviance: F(2, 26) = 7.86, p < .003, ε = 0.71): Large deviants evoked significantly greater responses than small deviants (t(13) = 2.89, p-fdr < .02) and intermediate deviants (t(13) = 3.13, p-fdr < .02).
- Superior Temporal Gyri:
    - **Left STG** (Significant effect of Deviance: F(2, 26) = 6.73, p-GG < .02, ε = 0.59): Large deviants evoked significantly greater responses than small deviants (t(13) = 2.74, p-fdr < .04) and intermediate deviants (t(13) = -2.59, p-fdr < .04).
    - **Right STG_1** (Significant effect of Deviance: F(2, 26) = 8.02, p < .002, ε = 0.84): Large deviants evoked significantly greater responses than small deviants (t(13) = 2.81, p-fdr < .03) and intermediate deviants (t(13) = 3.44, p-fdr < .02).
    - **Right STG_2** (Significant effect of Deviance: F(2, 26) = 6.78, p < .005, ε = 0.85): Large deviants evoked significantly greater responses than small deviants (t(13) = 2.38, p-fdr < .05) and intermediate deviants (t(13) = 3.55, p-fdr < .01).
- Frontal Opercula:
    - **Left FrOper** (Significant effect of Deviance: F(2, 26) = 7.16, p < .004, ε = 0.69): Large deviants evoked significantly greater responses than small deviants (t(13) = 2.54, p-fdr < .04) and intermediate deviants (t(13) = 3.22, p-fdr < .02).
    - **Right FrOper** (Significant effect of Deviance: : F(2, 26) = 4.33, p < .03, ε = 0.98): Large deviants evoked significantly greater responses than small deviants (t(13) = 2.41, p-fdr < .05) and intermediate deviants (t(13) = 2.65, p-fdr < .05).
- Inferior Frontal Gyrus – Pars Opercularis (Left Hemisphere):
    - **Left IFG oper_2** (Significant effect of Deviance: F(2, 26) = 5.36, p < .02, ε = 0.99): Large deviants evoked significantly greater responses than small deviants (t(13) = 2.52, p-fdr < .04) and intermediate deviants (t(13) = 3.16, p-fdr < .03).

- Insula (Left Hemisphere):
    - **Left Insula** (Significant effect of Deviance: $F(2, 26) = 9.09$, p-GG $< .006$, $\varepsilon = 0.61$): Large deviants evoked significantly greater responses than small deviants ($t(13) = 3.12$, p-fdr $< .02$) and intermediate deviants ($t(13) = 3.13$, p-fdr $< .02$).

Based on the power estimates (see Table A6), reliable MMN effects were identified in the following regions: Left HG_1, Left HG_2, Right HG, Left SMG, Left STS1_2, Right STG_1, Right STG_2, Left Frontal Operculum, Left IFG oper_2, and Left Insula. These regions consistently exhibited robust effects in both the ANOVA and the paired t-test for at least one contrast (Large vs. Small or Large vs. Intermediate), indicating stable and consistent neural responses to auditory deviants across conditions.

In contrast, regions such as the Right SMG, Left STS1_1, Left STG, and Right Frontal Operculum did not meet the reliability criterion, as power estimates remained below 0.8 in both comparisons. These areas thus showed weaker or less consistent MMN effects.

In Figure 9, we distinguish between ROIs with high and low statistical power. Only regions meeting the statistical reliability criterion are accompanied by plots of the source time courses (STCs) for each deviance condition.

Effects of Deviance and Cortical ROI on Late MMN/N2 Amplitudes (260–420 ms)

It is important to note that, in the late MMN/N2 time window (260–420 ms), neither the main effect of Deviance nor the Deviance × ROI interaction reached significance. Furthermore, no Deviance-related effects were observed in the control regions located bilaterally in the visual cortex.

In sum, EEG source analyses revealed significant early MMN-related deviance effects bilaterally in the supratemporal plane, including Heschl’s gyrus. Additional effects were observed in the left temporo-parietal cortex (supramarginal gyrus), superior temporal sulcus, frontal regions (including the frontal operculum and pars opercularis of the inferior frontal gyrus), and the insula, as well as in the right superior temporal gyrus. No deviance-related activity was detected during the late MMN/N2 time window, and no activation was observed in the visual control regions.

EEG

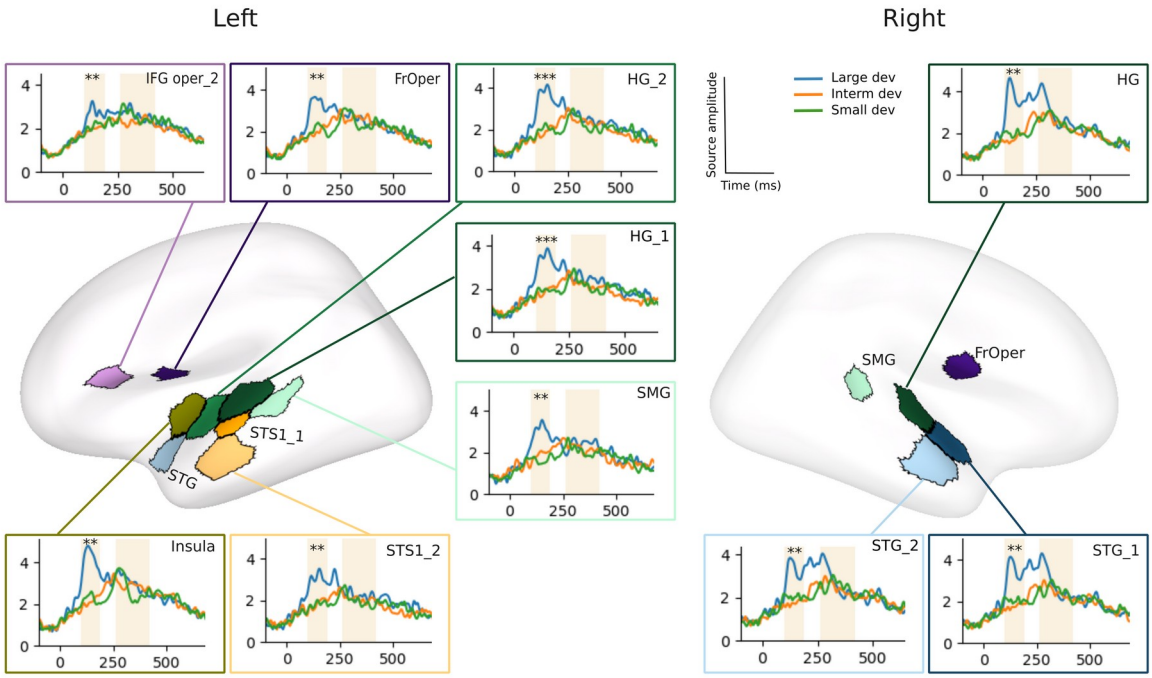

Figure 9. [Legend goes there]

3.2.2. MEG

Effects of Deviance and Cortical ROI on Early MMNm Amplitudes (100–190 ms)

For the early MMNm time window, two-way repeated-measures ANOVAs revealed a significant main effect of Deviance ($F(2, 26) = 23.57$, $p < .0001$, $\varepsilon = 0.64$), a significant main effect of ROI ($F(16, 208) = 15.09$, p-GG $< .0001$, $\varepsilon = 0.28$), and a significant Deviance × ROI interaction ($F(32, 416) = 5.28$, p-GG $< .009$, $\varepsilon = 0.07$). These findings indicate that MMNm amplitude varied as a function of both deviance level and cortical region.

Post-hoc power analyses confirmed that statistical power was high across all effects tested: Power (Deviance) > 0.99, Power (ROI) > 0.99, and Power (Interaction) = 0.98. This suggests that the sample size was sufficient to reliably detect the observed effects in the early MMNm time window.

To further examine the Deviance × ROI interaction, separate one-way repeated-measures ANOVAs were conducted for each ROI, with Deviance as a within-subject factor. Post-hoc

pairwise comparisons between deviance conditions were performed using paired-sample t-tests, corrected for multiple comparisons using FDR.

Significant effects of Deviance—characterized by stronger MMNm responses to large compared to both small and intermediate deviant stimuli—were observed in several cortical regions:

- Supratemporal Planes:
    - **Left Heschl's Gyrus** (HG_1, Significant effect of Deviance: F(2, 26) = 10.42, p-GG < .006, ε = 0.55): Large deviants evoked significantly greater responses than small deviants (t(13) = 3.32, p-fdr < .01) and intermediate deviants (t(13) = 3.25, p-fdr < .01).
    - **Left Heschl's Gyrus** (HG_2, Significant effect of Deviance: F(2, 26) = 13.06, p-GG < .003, ε = 0.56): Large deviants evoked significantly greater responses than small deviants (t(13) = 3.74, p-fdr < .005) and intermediate deviants (t(13) = 3.62, p-fdr < .005).
    - **Right Heschl's Gyrus** (HG; Significant effect of Deviance: F(2, 26) =14.74 , p < .002, ε = 0.58): Large deviants evoked significantly greater responses than small deviants (t(13) = 3.82, p-fdr < .004) and intermediate deviants (t(13) = 4.08, p-fdr < .004).
- Supramarginal Gyrus (Right hemisphere):
    - **Right SMG** (Significant effect of Deviance: F(2, 26) = 6.50, p-GG < .03, ε = 0.54). Large deviants evoked significantly greater responses than small deviants (t(13) = 3.24, p-fdr < .02) while the difference between large and intermediate deviants showed a trend toward significance (t(13) = 2.28, p-fdr = .06).
- Superior Temporal Gyri:
    - **Left STG** (Significant effect of Deviance: F(2, 26) = 8.02, p < .002, ε = 0.71). Large deviants evoked significantly greater responses than small deviants (t(13) = 2.76, p-fdr < .03) and intermediate deviants (t(13) = 3.57, p-fdr < .02).
    - **Right STG_2** (Significant effect of Deviance: F(2, 26) = 5.44, p < .02, ε = 0.87). Large deviants evoked significantly greater responses than small deviants (t(13) = 2.83, p-fdr < .03) and intermediate deviants (t(13) = 3.30, p-fdr < .02).
- Frontal Opercula:
    - **Left FrOper** (Significant effect of Deviance: F(2, 26) = 12.13, p-GG < .003, ε = 0.57). Large deviants evoked significantly greater responses than small deviants (t(13) = 3.68, p-fdr < .007) and intermediate deviants (t(13) =

3.44, p-fdr < .007).

- **Right FrOper** (Significant effect of Deviance: F(2, 26) = 14.51, p-GG < .001, ε = 0.61). Large deviants evoked significantly greater responses than small deviants (t(13) = 3.84, p-fdr < .004) and intermediate deviants (t(13) = 4.04, p-fdr < .004).

- Inferior Frontal Gyrus – Pars Opercularis (Left hemisphere):
  - **Left IFG oper_1** (Significant effect of Deviance: F(2, 26) = 9.78, p-GG < .007, ε = 0.55). Large deviants evoked significantly greater responses than small deviants (t(13) = 2.99 p-fdr < .02) and intermediate deviants (t(13) = 3.38, p-fdr < .02).
  - **Left IFG oper_2** (Significant effect of Deviance: F(2, 26) = 11.37, p < .0003, ε = 0.80). Large deviants evoked significantly greater responses than small deviants (t(13) = 3.34 p-fdr < .008) and intermediate deviants (t(13) = 4.52, p-fdr < .002).
- Insula (Left Hemisphere):
  - **Left Insula** (Significant effect of Deviance: F(2, 26) = 16.04, p < .0001, ε = 0.66). Large deviants evoked significantly greater responses than small deviants (t(13) = 4.20 p-fdr < .002) and intermediate deviants (t(13) = 4.23, p-fdr < .002).

Based on the power estimates (see Table A7), reliable MMNm effects were observed in the following brain regions: Left HG_1, Left HG_2, Right HG, Right SMG, Left STG, Right STG_2, the Left and Right Frontal Operculum, Left IFG oper_1, Left IFG oper_2, and the Left Insula. These regions exhibited statistical power greater than 0.8 in ANOVAs and t-test comparisons in at least one of the two condition contrasts (Large vs. Small or Large vs. Intermediate), indicating robust and consistent auditory mismatch responses. Notably, Left HG_2, Right HG, Left Insula, Right Frontal Operculum, and Left IFG oper_2 demonstrated particularly high power across both comparisons, suggesting especially strong and reliable effects in these areas.

All regions meeting the pre-established reliability threshold are in Figure 10, along with their corresponding plots of the source time courses (STCs) for each deviance condition.

Effects of Deviance and Cortical ROI on Late MMNm/N2m Amplitudes (260 to 420 ms)

Two-way repeated-measures ANOVAs conducted on the late MMNm/N2m time window revealed a significant main effect of Deviance ($F(2, 26) = 8.80$, $p < .002$, $\varepsilon = 0.95$), as well as a significant main effect of ROI ($F(16, 208) = 13.38$, p-GG $< .0001$, $\varepsilon = 0.29$). The interaction between Deviance and ROI did not reach significance ($F(32, 416) = 1.42$, p uncorrected = 0.068, p-GG = .23, $\varepsilon = 0.15$). Post-hoc statistical power was excellent for the main effects (Deviance: > 0.99; ROI: > 0.99), and moderate for the interaction term (0.8).

To further explore the Deviance × ROI interaction, one-way repeated-measures ANOVAs with Deviance as a within-subject factor were conducted separately for each ROI. Post-hoc pairwise comparisons between Deviance conditions were performed using paired-sample t-tests with an FDR-correction for multiple comparisons.

Significant Deviance effects—reflected by a stronger late MMNm/N2m response to large deviant stimuli—were observed in a more restricted set of regions:

- Supratemporal Plane (Left hemisphere):
    - **Left Heschl's Gyrus** (HG_1, Significant effect of Deviance: $F(2, 26) = 4.56$, $p < .02$, $\varepsilon = 0.95$). Large deviants evoked significantly greater responses than intermediate deviants ($t(13) = 2.87$, p-fdr $< .04$). The difference between large and small deviants was not significant ($t(13) = 0.96$ p-fdr = .35)
- Superior Temporal Gyrus (Right hemisphere):
    - **Right STG_1** (Significant effect of Deviance: $F(2, 26) = 4.33$, $p < .03$, $\varepsilon = 0.98$). Large deviants evoked significantly greater responses than small deviants ($t(13) = 3.05$ p-fdr $< .03$). The difference between large and intermediate deviants did not reach significance ($t(13) = 1.95$, p-fdr = .11).

According to the power estimates (see Table A8), reliable late MMNm/N2m effects were observed in Right STG_1, where both the ANOVA and the paired t-test comparison for the Large vs. Small contrast yielded statistical power above 0.8. In contrast, Left HG_1 did not meet the reliability criterion. These results suggest a robust and consistent late MMNm/N2m response in Right STG_1, whereas the evidence for Left HG_1 remains less conclusive.

The MMNm/N2m source time courses (STCs) for each deviance condition in these regions are presented in Figure 10.

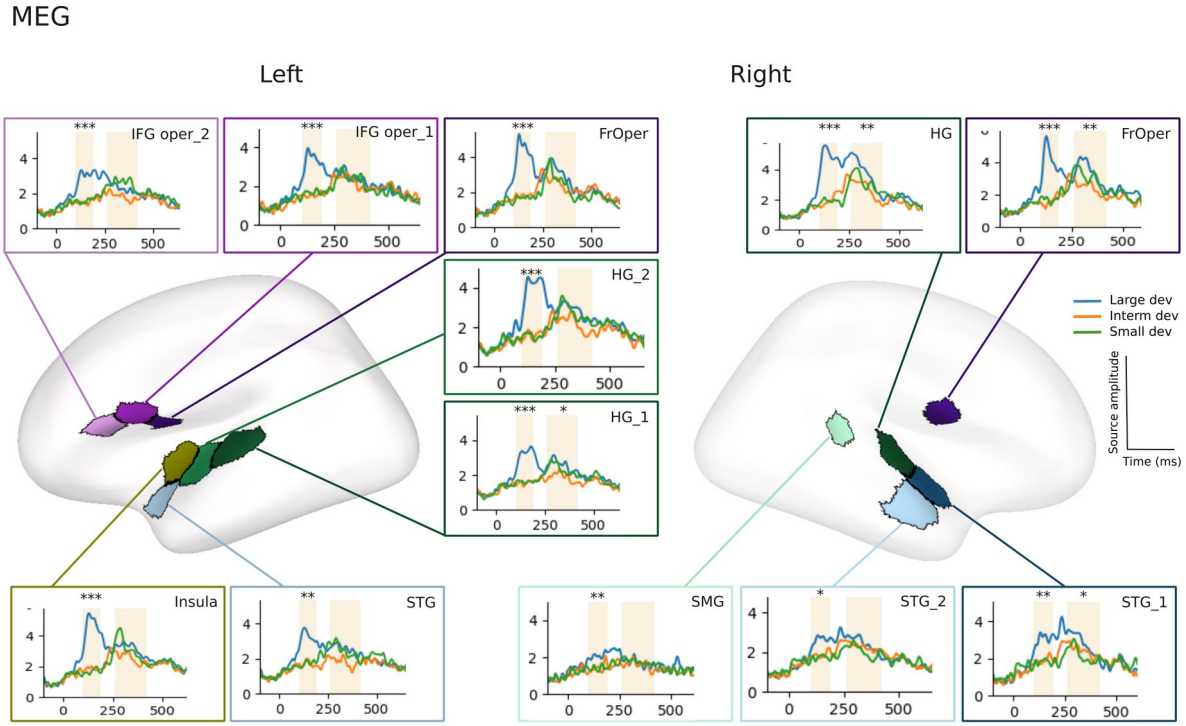

Figure 10. [Legend goes there]

As shown in Figures 9 and 10, large deviants elicited a clear peak of activity in several regions across both the left and right hemispheres, corresponding to the early MMN/MMNm (100–190 ms). This response was more pronounced with MEG than with EEG. Furthermore, while EEG did not reveal a distinct late MMN/N2 component, such a late response to large deviants was observable with MEG in the right superior temporal gyrus (STG_1).

4 Discussion

With this study, we aimed to compare how EEG and MEG capture the auditory MMN and MMNm to frequency deviant stimuli. EEG and MEG are two of the most widely used methods for studying human brain temporal dynamics. Moreover, the MMN signature is of particular interest for cognitive science and clinical research. Better understanding of the similarities and differences between EEG and MEG in this context will help inform interpretations of existing literature as well as methodological choices for future research. The originality of our study is in our use of simultaneously recorded empirical data and equivalent analysis of EEG and MEG data at sensor and source levels. We focused on comparing the latency, amplitude, and scalp distribution of early and late negative components as well as on determining how well our EEG and MEG data matched previously defined MMN and MMNm generators in frontal and supratemporal areas.

While the initial focus was on MMN and MMNm components, it is important to note that the late negative component we observed in both EEG and MEG could be interpreted as a late MMN/MMNm component or an N2 component. Earlier theoretical reviews (Näätänen et al. 2004; Folstein and Van Petten 2008) have already discussed the overlap between late negativity and N2/N2m components, suggesting that such responses may reflect sustained or elaborated change detection beyond automatic mismatch processing. Complex auditory pattern paradigms are known to elicit a late MMN or late discriminative negativity, with latencies often extending toward 400–500 ms, especially in rule-based or sequential pitch manipulations (e.g., (Recasens and Uhlhaas 2017). A recent local–global oddball design further supports the presence of distinct early and late MMN subcomponents: the early component may reflect local prediction error in central-frontal regions, while the later subcomponent is more frontal and may index global sequence irregularities (late MMN), potentially involving right prefrontal generators (Huang et al. 2024).

Our results, which reveal both early and late negativities (with the exception of late negativities in EEG from cortical ROI), are consistent with previous findings. However, the late negativity may also correspond to an N2/N2m component, reflecting controlled processing of pitch deviance (Tomé et al. 2015). While these two interpretations remain difficult to disentangle, the key point for present purposes is that results highlight the similarity of these components as recorded with EEG and MEG, despite some differences discussed below.

At the sensor level, we found that both EEG and MEG captured the early and late negative components with comparable latencies and amplitudes, lthough effect sizes were larger in MEG than in EEG. Moreover, there were differences in scalp distribution —fronto-central in EEG and centro-parietal in MEG—likely reflecting the distinct sensitivities of electrical and magnetic fields.

At the source level, results with both EEG and MEG were consistent with the fronto-temporal networks described in the literature (Phillips et al. 2015; Lecaignard et al. 2021). The specific comparisons between EEG and MEG source localization revealed interesting similarities and differences.

Regarding the observed similarities, the early MMN generators were consistently identified bilaterally by EEG and MEG within the supratemporal plane, encompassing Heschl’s gyri, the superior temporal gyri (STG), and the frontal opercula. On the left hemisphere, similar activations were notably localized in the pars opercularis of the inferior frontal gyrus (IFG oper 2) as well as in the insular cortex. On the right hemisphere, comparable activations across methods were observed in the supramarginal gyrus. Moreover, no generator was found in the visual control regions. Regarding the between-method differences, MMN generators were exclusively found with EEG in the left

superior temporal sulci (STS1). Conversely, while no generator of the deviance effect was found for the late MMN/N2 component with EEG, MMNm/N2m generators were found with MEG, specifically over the right superior temporal gyrus (STG_1).

4.1 **Sensor-level comparisons between EEG and MEG**

Large frequency deviant stimuli elicited early MMN/MMNm (100-190 ms) and late MMN/MMNm/N2/N2m (260-420 ms). The early MMN and MMNm peak latencies are in line with the latency of the MMN to large deviant stimuli typically reported in the literature (100-200 ms; (Huotilainen et al. 1998). As previously noted, the presence of a late negative component was not predicted, but a review of the literature showed that such a late effect has previously been named a “late MMN” in EEG studies using tone stimuli differing in frequency (Schulte-Körne et al. 2001) as well as in adults and children using vowel or sine wave tone stimuli, respectively (Korpilahti et al. 2001). In the latter study, late MMNs were interpreted as reflecting the “automatic processing of complex auditory stimuli.” In line with this interpretation, our results revealed that intermediate and small frequency deviant stimuli only elicited late MMN and MMNm components, possibly because they were more difficult to automatically detect than large frequency deviant stimuli.

In our study, we observed a slight difference between the later negative deflection components recorded with EEG and MEG, with the MEG showing a more pronounced component in the left parietal region. This divergence may reflect modality-specific sensitivities, as MEG is particularly sensitive to tangential currents generated in the sulci (Hämäläinen et al. 1993). As mentioned above it is also possible that what we take for a late MMN/MMNm is an N2 component to be associated to higher cognitive processes. such as auditory working memory (Alain et al. 1998) or attention related processes (Shestakova et al. 2003). This interpretation should nonetheless be considered with caution, as the effects observed on the late component did not reach the threshold for statistical significance. Further studies involving a larger sample size will be necessary to confirm these findings.

As expected based on results of a previous study using the same stimuli (Frey et al. 2022), the main effect of deviance and the deviance x ROI interaction were significant in both the early and late time windows in EEG. By contrast, the main effect of deviance was not significant in either the early or late latency windows in MEG. This may indicate that the difference between large and intermediate or small deviant stimuli (i.e., the deviance effect) is more pronounced in EEG than in MEG, suggesting that EEG may be more

sensitive at sensor-level to the overall negative deflection associated with the late MMN component.

Moreover, while the deviance x ROI interaction was significant with both EEG and MEG, the scalp distribution of the early and late effects was quite different: more widespread over the scalp EEG electrodes and more focused across the MEG sensors. As reported in previous studies (Sams et al. 1985; Rinne et al. 2000; Näätänen et al. 2004), the early MMN was fronto-centrally distributed, with a clear polarity inversion between frontal and parietal electrodes over both the left and the right hemisphere (and no clear activity at left and right central sites). The scalp distribution was similar for the late MMN/N2 component. Moreover, the large frequency deviant stimuli were always associated with larger early and late effects than intermediate and small deviant stimuli, which did not significantly differ from one another. By contrast, while the same amplitude relationship was found with MEG (Large > Intermediate=Small), the magnetic fields for the early and late MMNm/N2m components resembled that of two symmetric equivalent dipoles located bilaterally (frontal, central and parietal).

Considering the differences in topographies intrinsic to the different properties of electrical and magnetic fields, performing direct comparisons at sensor-level is difficult. This is further complicated by the different units used to measure EEG (μV) and MEG (fT) signals. Thus, to better understand the strength of each method for measuring the mismatch response at the sensor level and to normalize results for comparison, we performed effect size analyses that revealed interesting findings (Figures 7 and 8). Comparing the effect sizes for electrodes and magnetometers for the early MMN/MMNm, we found that 62 out of 248 (25%) magnetometers were significant and nine had moderate effect sizes. By contrast, 12 out of 64 (19%) electrodes showed significant effects but none crossed the 0.5 threshold for moderate effect sizes. Results for the late MMN/MMNm/N2/N2m showed that no electrodes showed a significant difference for more than one participant, whereas 13 out of 248 (5%) magnetometers showed significant differences and small effect sizes. While it was not possible to make a one-to-one comparison of magnetometers and electrodes due to differences in field properties, this analysis served as a first step to further examine differences in EEG and MEG at the sensor level, a topic which has not yet been explored in literature.

4.2 **Source-level comparisons between EEG and MEG**

By analyzing simultaneously recorded EEG and MEG data, we gathered complementary information regarding the underlying generators of the auditory MMN/MMNm to large frequency deviant stimuli. This allowed us to more precisely address the fundamentally

ill-posed inverse problem. Going beyond the auditory MMN fronto-temporal networks, originally proposed by Näätänen and Michie (1979) and supported by results using either EEG (e.g., Rinne et al. 2000) or MEG (e.g., Levänen et al. 1996) source localization, our results revealed that, with both the EEG and MEG methods, the largest auditory early early MMN/MMNm and late MMN/MMNm/N2/N2m activity was generated bilaterally in the supratemporal plane – including Heschl's Gyrus, the superior temporal gyrus and the frontal operculum.

Clearly, these results, gained from both methods, support the implication of these brain regions in the generation of the auditory early and late effects elicited by frequency deviant stimuli (Fitzgerald and Todd 2020; Lecaignard et al. 2021). Finally, it is also important to note that these results are strengthened by the fact that no significant activity was found in the left and right visual areas that served as control regions.

Interestingly for the main objective of our study, EEG and MEG also revealed different potential generators of the early MMN/MMNm and late /MMN/MMNm/N2/N2m. First, the left superior temporal sulcus (posterior) region was identified as an MMN generator based on EEG data but not based on MEG data. Similar results were reported by Lecaignard et al (2021). It t is striking that, in two independent studies, using different EEG systems and stimuli, this region was identified as an MMN generator based on EEG but not on MEG data. It is possible that these findings result from more leakage in EEG than in MEG, with close regions, such as the STS, being "contaminated" in EEG but not in MEG, by a potential main generator located in the STG. Another, more likely, interpretation is that the generator specifically activated by automatic pitch processing and located in the left superior temporal gyrus is radially oriented relative to the scalp surface such that it can be detected with EEG but not with MEG. Importantly, this finding would confirm the widespread idea that EEG is sensitive to more brain sources - those that are both radially and tangentially oriented relative to the surface of the scalp - than MEG, which is only sensitive to tangentially oriented sources (Puce and Hämäläinen 2017).

Second, significant deviance effects in the fronto-temporal network described above were only found for the early MMN with EEG but for both the early and late MMNm/N2m components with MEG, which may indicate that the time course of magnetic activity lasted longer than electric activity in these brain regions. Moreover, while the generators of the early MMNm were bilaterally distributed across both hemispheres—consistent with the MMN topography observed in EEG—the generators of the late MMNm/N2m showed the most reliable power in one of the superior temporal regions defined in the Schaefer atlas (right STG_1), located near Heschl's gyrus. This finding may be accounted for by an auditory processing asymmetry that remains undetected in EEG, possibly linked to the orientation of the underlying neural sources. The right auditory cortex is especially implicated in the processing of global acoustic structures and slow temporal modulations,

as has been consistently demonstrated in functional imaging studies (Zatorre and Belin 2001).

4.3 **Limitations and Conclusion**

A clear limitation of the present study is the small sample size (N = 14 participants), which reflects the technical and logistical constraints of simultaneous EEG–MEG recordings. This type of dual acquisition presents numerous challenges, such as the need for precise synchronization between systems, magnetic and electrical interference, increased constraints on participant movements, and equipment compatibility issues. As a result, data from a substantial number of participants (N = 7) could not be included in the analyses. Consequently, the findings reported here should be interpreted with caution and will require replication in future studies.

Another limitation of the present work concerns the downsampling of the source space to 516 vertices (with free dipole orientation) across the cortical surface, a choice made to reduce computational demands. This inevitably constrains the spatial resolution of the source estimates and of the associated regions of interest, which should be refined in future studies.

A further limitation relates to the interpretation of divergent findings between EEG and MEG. For example, while the left superior temporal sulcus was identified as an MMN generator based on EEG data, no such generator was observed in this region with MEG data. The reasons for these discrepancies remain speculative, and additional experiments will be required to clarify this issue. Importantly, similar EEG–MEG differences have already been reported by Lecaignard et al. (2021) using different recording systems, which suggests that such divergences may reflect modality-specific sensitivities rather than methodological artifacts.

Despite theses limitations, the present results provide valuable insights into the complementarity of EEG and MEG. Pre-attentive processing of harmonic complex sounds varying in frequency elicited both early MMN/MMNm and late MMN/MMNm/N2/N2m components. In sensor level analyses, these components showed similar temporal dynamics across the two methods, with both early and late responses reliably identified in EEG and MEG. However, while the main effect of deviance (i.e., the difference between large and intermediate or small deviant stimuli) was significant in both the early and late time windows in EEG, it was not significant in either windows in MEG, possibly revealing greater sensitivity or less variability in EEG than in MEG at sensor level.

Source localization analyses revealed similar results in EEG and in MEG, with generators in the superior temporal gyrus, in the Heschl's gyrus, in the Frontal Operculum, in the inferior frontal regions (pars opercularis), and in the insular regions. Notably, neither the early MMN/MMNm nor the late MMN/MMNm/N2/N2m responses were observed in visual control regions with either method.

One of the most striking differences in favor of EEG and in line with previous literature (e.g., (Puce and Hämäläinen 2017), was the illustration that EEG tended to be sensitive to more brain sources of activity than MEG (sources located in the left superior temporal sulcus were detected by EEG but not by MEG). This differential sensitivity of EEG and MEG to underlying sources of brain activity may also possibly account for the differences in the scalp distribution of the deviance effect (fronto-central with EEG and centro-parietal with MEG). This may suggest that magnetic activity persists longer than electrical activity and that MEG is possibly more sensitive to weaker neural generators in these regions. This interpretation is supported by the higher signal-to-noise ratio observed in MEG compared to EEG, as indicated by larger effect sizes computed at the sensor level. However, this difference in effect sizes needs to be replicated in further studies.

In conclusion, and most importantly for our understanding of the anatomo-functional organization of pre-attentive pitch processing, both methods showed similar results, both at the sensor and at the source level of analysis but they also revealed differences that highlight their complementarity. EEG seems to reveal sources that are not detected with MEG (probably radially oriented sources relative to brain surface) and MEG may detect weaker sources of brain activity than EEG.

5 Acknowledgements

We thank all experiment participants, as well as Thomas Chehrerian and Marie Edet for their help with data recording and processing. We would also like to thank Françoise Lecaignard and colleagues for generously sharing their MEEG source localization data with us.

6 References

Alain C, Woods DL, Knight RT (1998) A distributed cortical network for auditory sensory memory in humans. Brain Res 812:23–37. https://doi.org/10.1016/s0006-8993(98)00851-8

Areces-Gonzalez A, Paz-Linares D, Riaz U, et al (2024) CiftiStorm pipeline: facilitating reproducible EEG/MEG source connectomics. Front Neurosci 18:. https://doi.org/10.3389/fnins.2024.1237245
Atienza M, Cantero JL, Dominguez-Marin E (2002) Mismatch negativity (MMN): an objective measure of sensory memory and long-lasting memories during sleep. Int J Psychophysiol 46:215–225. https://doi.org/10.1016/S0167-8760(02)00113-7
Benjamini Y, Hochberg Y (1995) Controlling the False Discovery Rate: A Practical and Powerful Approach to Multiple Testing. J R Stat Soc Ser B Methodol 57:289–300
Cohen J (2013) Statistical Power Analysis for the Behavioral Sciences, 2nd edn. Routledge, New York
Colombet B, Woodman M, Badier JM, Bénar CG (2015) AnyWave: A cross-platform and modular software for visualizing and processing electrophysiological signals. J Neurosci Methods 242:118–126. https://doi.org/10.1016/j.jneumeth.2015.01.017
Dale AM, Liu AK, Fischl BR, et al (2000) Dynamic statistical parametric mapping: combining fMRI and MEG for high-resolution imaging of cortical activity. Neuron 26:55–67. https://doi.org/10.1016/s0896-6273(00)81138-1
Fitzgerald K, Todd J (2020) Making Sense of Mismatch Negativity. Front Psychiatry 11:. https://doi.org/10.3389/fpsyt.2020.00468
Folstein JR, Van Petten C (2008) Influence of cognitive control and mismatch on the N2 component of the ERP: A review. Psychophysiology 45:152–170. https://doi.org/10.1111/j.1469-8986.2007.00602.x
Frey A, Barbaroux M, Dittinger E, Besson M (2022) Effects of Psychoacoustic Training on the Pre-Attentive Processing of Harmonic Sounds and Syllables. J Speech Lang Hear Res 65:2003–2015. https://doi.org/10.1044/2022_JSLHR-21-00441
Giard M-H, Perrin F, Pernier J, Bouchet P (1990) Brain Generators Implicated in the Processing of Auditory Stimulus Deviance: A Topographic Event-Related Potential Study. Psychophysiology 27:627–640. https://doi.org/10.1111/j.1469-8986.1990.tb03184.x
Glasser MF, Coalson TS, Robinson EC, et al (2016) A multi-modal parcellation of human cerebral cortex. Nature 536:171–178. https://doi.org/10.1038/nature18933
Gramfort A, Luessi M, Larson E, et al (2013) MEG and EEG data analysis with MNE-Python. Front Neurosci 7:. https://doi.org/10.3389/fnins.2013.00267
Gupta S, Bhardwaj A (2022) Mismatch Negativity Responses to Different Auditory Attributes in Normally Developing Infants and Children. Cureus. https://doi.org/10.7759/cureus.33163
Hämäläinen M, Hari R, Ilmoniemi RJ, et al (1993) Magnetoencephalography---theory, instrumentation, and applications to noninvasive studies of the working human brain. Rev Mod Phys 65:413–497. https://doi.org/10.1103/RevModPhys.65.413
Hari R (1990) Magnetic Evoked Fields of the Human Brain: Basic Principles and Applications. In: Rossini PM, Mauguière F (eds) New Trends and Advanced Techniques in Clinical Neurophysiology. Elsevier, pp 3–12
Houck JM, Claus ED (2020) A comparison of automated and manual co-registration for magnetoencephalography. PLOS ONE 15:e0232100. https://doi.org/10.1371/journal.pone.0232100
Huang YT, Wu C-T, Koike S, Chao ZC (2024) Dissecting Mismatch Negativity: Early and Late Subcomponents for Detecting Deviants in Local and Global Sequence Regularities. eNeuro 11:ENEURO.0050-24.2024. https://doi.org/10.1523/ENEURO.0050-24.2024
Huotilainen M, Winkler I, Alho K, et al (1998) Combined mapping of human auditory EEG and MEG responses. Electroencephalogr Clin Neurophysiol 108:370–379. https://doi.org/10.1016/s0168-5597(98)00017-3
Kong R, Yang Q, Gordon E, et al (2021) Individual-Specific Areal-Level Parcellations Improve Functional Connectivity Prediction of Behavior. Cereb Cortex N Y NY 31:4477–4500. https://doi.org/10.1093/cercor/bhab101
Korpilahti P, Krause CM, Holopainen I, Lang AH (2001) Early and Late Mismatch Negativity Elicited by Words and Speech-Like Stimuli in Children. Brain Lang 76:332–339. https://doi.org/10.1006/brln.2000.2426
Lecaignard F, Bertrand O, Caclin A, Mattout J (2021) Empirical Bayes evaluation of fused EEG-MEG source reconstruction: Application to auditory mismatch evoked

responses. NeuroImage 226:117468. https://doi.org/10.1016/j.neuroimage.2020.117468
Levänen S, Ahonen A, Hari R, et al (1996) Deviant auditory stimuli activate human left and right auditory cortex differently. Cereb Cortex N Y N 1991 6:288–296. https://doi.org/10.1093/cercor/6.2.288
Lin F-H, Witzel T, Ahlfors SP, et al (2006) Assessing and improving the spatial accuracy in MEG source localization by depth-weighted minimum-norm estimates. NeuroImage 31:160–171. https://doi.org/10.1016/j.neuroimage.2005.11.054
Näätänen R, Gaillard AW, Mäntysalo S (1978) Early selective-attention effect on evoked potential reinterpreted. Acta Psychol (Amst) 42:313–329. https://doi.org/10.1016/0001-6918(78)90006-9
Näätänen R, Michie PT (1979) Early selective-attention effects on the evoked potential: A critical review and reinterpretation. Biol Psychol 8:81–136. https://doi.org/10.1016/0301-0511(79)90053-X
Näätänen R, Pakarinen S, Rinne T, Takegata R (2004) The mismatch negativity (MMN): towards the optimal paradigm. Clin Neurophysiol 115:140–144. https://doi.org/10.1016/j.clinph.2003.04.001
Neuhoff N, Bruder J, Bartling J, et al (2012) Evidence for the Late MMN as a Neurophysiological Endophenotype for Dyslexia. PLOS ONE 7:e34909. https://doi.org/10.1371/journal.pone.0034909
Phillips HN, Blenkmann A, Hughes LE, et al (2015) Hierarchical Organization of Frontotemporal Networks for the Prediction of Stimuli across Multiple Dimensions. J Neurosci 35:9255–9264. https://doi.org/10.1523/JNEUROSCI.5095-14.2015
Puce A, Hämäläinen MS (2017) A Review of Issues Related to Data Acquisition and Analysis in EEG/MEG Studies. Brain Sci 7:58. https://doi.org/10.3390/brainsci7060058
Recasens M, Uhlhaas PJ (2017) Test-retest reliability of the magnetic mismatch negativity response to sound duration and omission deviants. NeuroImage 157:184–195. https://doi.org/10.1016/j.neuroimage.2017.05.064
Reuter M, Schmansky NJ, Rosas HD, Fischl B (2012) Within-subject template estimation for unbiased longitudinal image analysis. NeuroImage 61:1402–1418. https://doi.org/10.1016/j.neuroimage.2012.02.084
Rinne T, Alho K, Ilmoniemi RJ, et al (2000) Separate Time Behaviors of the Temporal and Frontal Mismatch Negativity Sources. NeuroImage 12:14–19. https://doi.org/10.1006/nimg.2000.0591
Sams M, Paavilainen P, Alho K, Näätänen R (1985) Auditory frequency discrimination and event-related potentials. Electroencephalogr Clin Neurophysiol Potentials Sect 62:437–448. https://doi.org/10.1016/0168-5597(85)90054-1
Schaefer A, Kong R, Gordon EM, et al (2018) Local-Global Parcellation of the Human Cerebral Cortex from Intrinsic Functional Connectivity MRI. Cereb Cortex 28:3095–3114. https://doi.org/10.1093/cercor/bhx179
Scherg M, Vajsar J, Picton TW (1989) A Source Analysis of the Late Human Auditory Evoked Potentials. J Cogn Neurosci 1:336–355. https://doi.org/10.1162/jocn.1989.1.4.336
Schoffelen J-M, Hultén A, Lam N, et al (2017) Frequency-specific directed interactions in the human brain network for language. Proc Natl Acad Sci 114:8083–8088. https://doi.org/10.1073/pnas.1703155114
Schulte-Körne G, Deimel W, Bartling J, Remschmidt H (2001) Speech perception deficit in dyslexic adults as measured by mismatch negativity (MMN). Int J Psychophysiol 40:77–87. https://doi.org/10.1016/S0167-8760(00)00152-5
Ségonne F, Dale AM, Busa E, et al (2004) A hybrid approach to the skull stripping problem in MRI. NeuroImage 22:1060–1075. https://doi.org/10.1016/j.neuroimage.2004.03.032
Shestakova A, Huotilainen M, Čeponien≐ R, Cheour M (2003) Event-related potentials associated with second language learning in children. Clin Neurophysiol 114:1507–1512. https://doi.org/10.1016/S1388-2457(03)00134-2
Tait L, Özkan A, Szul MJ, Zhang J (2021) A systematic evaluation of source reconstruction of resting MEG of the human brain with a new high-resolution atlas: Performance, precision, and parcellation. Hum Brain Mapp 42:4685–4707. https://doi.org/10.1002/hbm.25578

Takahashi H, Rissling AJ, Pascual-Marqui R, et al (2013) Neural substrates of normal and impaired preattentive sensory discrimination in large cohorts of nonpsychiatric subjects and schizophrenia patients as indexed by MMN and P3a change detection responses. NeuroImage 66:594–603. https://doi.org/10.1016/j.neuroimage.2012.09.074

Todd J, Michie PT, Schall U, et al (2012) Mismatch negativity (MMN) reduction in schizophrenia—Impaired prediction-error generation, estimation or salience? Int J Psychophysiol 83:222–231. https://doi.org/10.1016/j.ijpsycho.2011.10.003

Tomé D, Barbosa F, Nowak K, Marques-Teixeira J (2015) The development of the N1 and N2 components in auditory oddball paradigms: a systematic review with narrative analysis and suggested normative values. J Neural Transm Vienna Austria 1996 122:375–391. https://doi.org/10.1007/s00702-014-1258-3

Umbricht D, Koller R, Schmid L, et al (2003) How specific are deficits in mismatch negativity generation to schizophrenia? Biol Psychiatry 53:1120–1131. https://doi.org/10.1016/S0006-3223(02)01642-6

Vallat R (2018) Pingouin: statistics in Python. J Open Source Softw 3:1026. https://doi.org/10.21105/joss.01026

Zatorre RJ, Belin P (2001) Spectral and temporal processing in human auditory cortex. Cereb Cortex N Y N 1991 11:946–953. https://doi.org/10.1093/cercor/11.10.946

7 Figure legends

Figure 1. Regions of interest (ROIs) used for EEG and MEG analyses. For EEG analysis (A), ROIs were selected from a 64-electrode cap template based on the 10-20 system. For MEG analysis (B), ROIs were selected from a 248 magnometer system template. They were chosen to match the positions of EEG ROIs as closely as possible. For both EEG and MEG, the following 9 ROIs were used for analyses: Frontal Left, Frontal Midline, and Frontal Right in pink; Central Left, Central Midline, and Central Right in purple/blue; Parietal Left, Parietal Midline, and Parietal Right in green.

Figure 2. Illustration of Event-Related Potentials (top) and Event-Related Fields (bottom) across subjects (n=14). Early MMN (100-190 ms) and late MMN/N2 components (260-420 ms) to large deviant stimuli are illustrated with all channels superimposed. The two latency windows are highlighted in light orange. In green, representations of the Global Field Power (GFP) for EEG and of the Root Mean Square (RMS) for MEG.

Figure 3. Topographical maps across subjects (n=14) for EEG (top) and MEG (bottom) in response to large deviant stimuli. Maps are represented for two latency windows that correspond to the early MMNs (100- 190 ms) and late MMNs/N2s (260-420 ms) MMN/MMNm components.

Figure 4. The ROIs were superimposed onto the cortical reconstruction of the left and right template brain: (1) the Superior Temporal (ST) regions are colored in green for gyri and in orange for sulci, (2) the Inferior Frontal regions in purple, (3) the Insular regions in blue, and (4) the Visual regions in red (see Table A1 for details) [HG= Heschl’s Gyrus; SMG= Supramarginal Gyrus; STG= Superior Temporal Gyrus; STS= Superior Temporal Sulcus; IFG oper= Inferior Frontal Gyrus pars opercularis; Vis = Visual Cortex].

Figure 5. At Fronto-Central ROIs, and in two-time windows, highlighted in light orange,

large deviant stimuli elicited larger early MMN (100-190 ms) and late MMN/N2 components (260-420 ms) compared to intermediate and small deviants. Significant p-values are indicated with a star (*: p< .05, **: p< .01, ***: p< .001).

Figure 6. At Centro-Parietal ROIs, and in two-time windows, highlighted in light orange, large deviant stimuli elicited larger early MMNm (100-190 ms) and late MMNm/N2m components than intermediate and small deviants. Significant p-values are indicated with a star (*: p< .05, **: p< .01, ***: p< .001).

Figure 7. EEG effect-size amplitudes for the early MMN component across the significant channels (left, represented at scalp locations and right, listed on the x-axis). A moderate effect size is indicated by a dashed line (0.5 threshold).

Figure 8. MEG effect-size amplitudes for the early MMNm (top) and late MMNm/N2m (bottom) components across the significant sensors (left, spatial representations relative to the scalp and right, listed on the x-axis). A moderate effect size is indicated by the dashed line (0.5 threshold).

Figure 9. EEG source-level results. Only regions of interest (ROIs) showing a significant deviance effect for the early MMN or late MMN/N2 components are displayed on the cortical reconstruction of the left and right template brains. The corresponding source time courses (amplitude on the y-axis, time in milliseconds on the x-axis) are shown only for ROIs where sufficient statistical power (≥ 0.80) was reached in both the ANOVAs and one of the two post-hoc pairwise comparisons (large vs. small; large vs. Intermediate).

Figure 10. MEG source-level results. Only ROIs showing a significant deviance effect for the early MMNn or late MMNm/N2m components are displayed on the cortical reconstruction of the left and right template brains. The corresponding source time courses (amplitude on the y-axis, time in milliseconds on the x-axis) are shown only for ROIs where sufficient statistical power (≥ 0.80) was reached in both the ANOVAs and one of the two post-hoc pairwise comparisons (large vs. small; large vs. Intermediate).

Figure A1**.** Group-averaged dSPM source maps of early (130 ms) and late (190 ms) responses for the Large Deviant – Standard contrast, projected onto the standardized cortical surface (*fsaverage*), averaged across all 14 subjects. Column 1 shows EEG activity, column 2 shows MEG activity. Rows alternate between the left (L) and right (R) hemispheres. The upper half of the panel corresponds to 130 ms, and the lower half to 190 ms.

Figure A2. Visualization of ROIs and source space on the fsaverage brain template. The inflated cortical surface of both hemispheres from the standard subject fsaverage is displayed, showing the current set of ROIs. Black dots indicate the source space vertices used for MEG/EEG source reconstruction, based on an oct4 spacing. This visualization helps evaluate the spatial correspondence between the defined ROIs and the distributed source model.

8 Appendix

8.1 Illustration of dSPM statistical maps projected onto the cortical surface

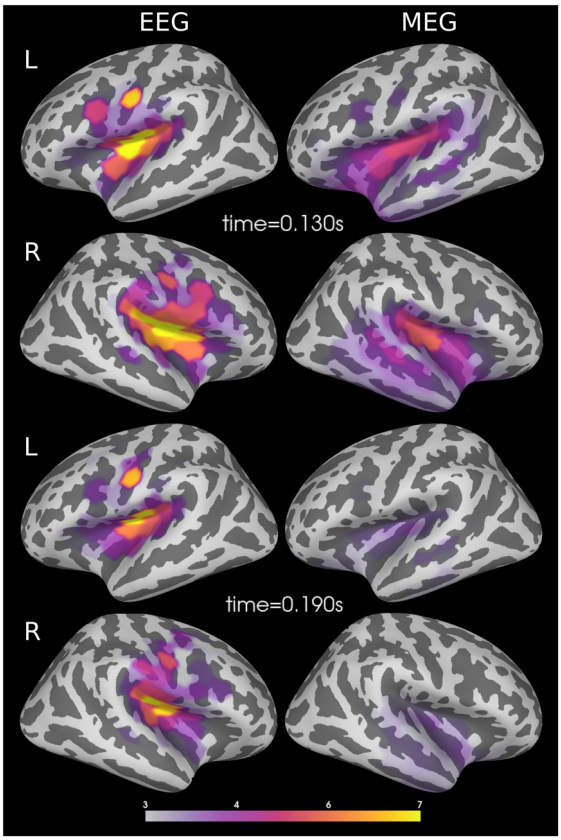

Figure A1. [Legend goes there]

8.2 Definition of ROIs in Source-Level Analysis

8.2.1. Correspondence between peak MNI coordinates and ROI names

Table A1. The Regions of Interest (ROIs) were defined based on the peak coordinates of clusters associated with the Mismatch Negativity (MMN) component, kindly provided by

Françoise Lecaignard and colleagues. Our analysis specifically focused on the condition involving frequency deviant stimuli within the 150–200 milliseconds latency window (see Figure 3 from (Lecaignard et al. 2021)). The peak locations were provided in Montreal Neurological Institute (MNI) coordinates (X, Y, Z in millimetres). To facilitate interpretation and integration into our current analysis, these coordinates were mapped onto the Schaefer et al. (Schaefer et al. 2018) using an in-house Python code (see Appendix, section 9.3) and Ebrains (https://atlases.ebrains.eu) brain atlases and assigned simplified labels. [LH= Left Hemisphere; RH= Right Hemisphere; HG= Heschl's Gyrus; SMG= Supramarginal Gyrus; STS= Superior Temporal Sulcus; IFG oper= Inferior Frontal Gyrus pars opercularis; Vis= Visual Cortex, IFG= Inferior Frontal Gyrus, STG= Superior Temporal Gyrus].

ROI Name			From Lecaignard			
Current Name	Schaefer Name	Ebrains	Tech	X	Y	Z
Left Hemisphere						
HG_1	LH_Aud_ST_3	Area Te 1.0 (HESCHL)	MEEG	-45	-23	7
HG_1	LH_Aud_ST_4	Area Te 2.1 (STG)	MEEG	-60	-9	2
HG_2	LH_Aud_ST_4	Area Te 1.1 (HESCHL)	MEG	-42	-20	6
HG_2	LH_Aud_ST_4	Area Te 1.2 (HESCHL)	MEG	-57	0	0
SMG	LH_Aud_ST_5	Area TPJ (STG, SMG)	EEG	-58	-40	10
STS1_1	LH_Aud_ST_7	Area STS1 (STS)	MEG	-60	-11	-2
STS1_2	LH_Aud_ST_4	Area STS1 (STS)	MEG	-50	-12	-7
STS1_2	LH_Language_Temp_3	Area STS1 (STS)	MEEG	-50	-6	-8
FrOper	LH_SalVenAttnA_FrOper_1	Area Op5 (Frontal Operculum)	MEEG	-53	-6	6
IFG oper_1	LH_SalVenAttnB_IFG_1	Area 6r1 (PreCG) / Area 44 (IFG)	MEEG	-56	6	9
IFG oper_2	LH_SalVenAttnB_IFG_1	Area 6r1 (PreCG) / Area 44 (IFG)	MEG	-53	10	15
Insula	LH_SalVenAttnA_Ins_3	Area Id3 (Insula)	EEG	-43	-18	-8
STG	LH_Aud_TempPole_1	Area TI (STG)	EEG	-46	-1	-14
STG	LH_Aud_TempPole_1	Area TI (STG)	MEG	-46	-3	-13
Vis	LH_VisualA_ExStr_4					
Right Hemisphere						
HG	RH_Aud_ST_2	Area Te 1.0 (HESCHL)	MEG	48	-17	6
HG	RH_Aud_ST_2	Area Te 1.0 (HESCHL)	MEEG	48	-19	6
HG	RH_SalVenAttnA_FrOper_1	Area Op4 / Te 1.2 (HESCHL)	MEEG	55	-5	4
SMG	RH_Aud_ST_4	Area TPJ (STG, SMG) right	EEG	60	-40	10
FrOper	RH_SalVenAttnA_FrOper_1	Area Op6 (Frontal Operculum)	MEEG	57	2	6
Insula	RH_SalVenAttnB_Ins_3	Area Id1 (Insula)	EEG	42	-17	-8
Insula	RH_SalVenAttnB_Ins_3	Area Id3 (Insula)	MEG	37	-12	-6
STG_1	RH_SalVenAttnA_Ins_3	Area TI (STG)	EEG	47	-1	-14
STG_1	RH_Aud_ST_3	Area TeI (STG)	MEG	49	-13	-2
STG_2	RH_Aud_ST_3	Area TI (STG)	MEG	49	-1	-13
STG_2	RH_Aud_ST_3	Area Te 3 (STG)	MEG	60	-4	-4
STG_2	RH_Aud_ST_3	Area TI (STG)	MEEG	49	-7	-8
Vis	RH_VisualA_ExStr_4					

8.2.2. Custom Python Code for Surface Projection

We provide a simple Python function designed to find the closest cortical surface vertex to a given MNI coordinate. The closest vertex was defined on the standardized cortical surface (FreeSurfer's fsAverage). Since the Schaefer atlas version used is defined in the same space, the corresponding Schaefer ROI name is then retrieved via the vertex index.

```
from scipy.spatial import cKDTree
import numpy as np

def find_closest_vertex(coords, mni_coord):
    """
    Find the surface vertex closest to a given MNI coordinate.
    Parameters
    ----------
    coords : ndarray, shape (n_vertices, 3)
        Array of 3D coordinates representing the cortical surface.
    mni_coord : array-like, shape (3,)
        Target MNI coordinate (in millimeters).

    Returns
    -------
    idx : int
        Index of the closest vertex in `coords`.
    dist : float
        Euclidean distance between the vertex and the target coordinate.
    """
    tree = cKDTree(coords)
    dist, idx = tree.query(mni_coord)
    return idx, dist
```

8.2.3. Spatial correspondence between the defined ROIs and the distributed source model

In Figure A2, which illustrates the spatial correspondence between the regions of interest (ROIs) and the distributed source model, we observe a mismatch for the right hemisphere ROI labeled Insula. Specifically, no source space vertices correspond to this ROI, indicating that it is not represented within the current source model. For this reason, we subsequently excluded this ROI from our study.

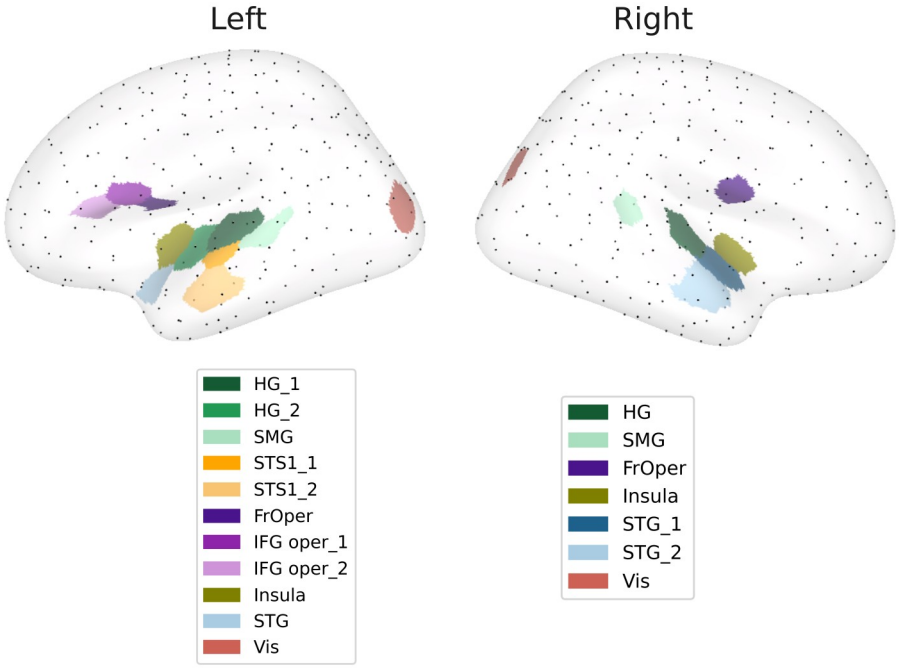

Figure A2. [Legend goes there]

8.3 Post-hoc power Estimation

8.3.1. Description

Post hoc Power Estimation for Repeated-measures ANOVA

To assess the sensitivity of our repeated-measures ANOVA, we estimated the statistical power for each main effect and interaction using the Python library Pingouin (`power_rm_anova()` function; Vallat 2018). This function calculates the post hoc power of a repeated-measures ANOVA based on the observed effect size (Partial Eta Squared, η^2), number of levels per factor (m), number of subjects (n), Greenhouse-Geisser correction (ε), within-subject correlation ($corr$), and the significance threshold (α).

Partial Eta Squared (η^2_p) values were estimated from the reported F-values and degrees of freedom (df) using the following formula:

$$\eta_p^2 = \frac{F \cdot df_{effect}}{(F \cdot df_{effect} + df_{error})}$$

Equation A1. [Equation goes there]

Post hoc Power Estimation for Paired *t*-tests

To estimate the post-hoc statistical power of significant pairwise comparisons, we used a simulation-based approach tailored for paired t-tests. The method accounts for intra-subject correlations and was implemented in Python. For each contrast, the observed t-value was converted into Cohen's d for paired samples using the formula:

$$d = \frac{t}{\sqrt{n}}$$

Equation A2. [Equation goes there]

where n is the number of subjects (here, n = 14).

To estimate power, we ran Monte Carlo simulations (10,000 iterations per contrast) using synthetic paired data sampled from a bivariate normal distribution. The two distributions had a specified mean difference equal to d, unit variance, and an assumed intra-subject correlation of ρ = 0.5 (a conservative assumption). In each iteration, a paired t-test was applied, and the proportion of simulations yielding $p < 0.05$ was taken as an empirical estimate of power. Below is a Python code snippet illustrating the simulation procedure:

```
# Simulate post hoc power for paired t-tests
def simulate_posthoc_power(d, n, rho=0.5, alpha=0.05, n_iter=10000):
    significant_results = 0
    cov = [[1, rho], [rho, 1]]
    for _ in range(n_iter):
        data = np.random.multivariate_normal(mean=[0, d], cov=cov, size=n)
        x, y = data[:, 0], data[:, 1]
        _, p_val = ttest_rel(x, y)
        if p_val < alpha:
            significant_results += 1
    return significant_results / n_iter
```

8.3.2. Results (Tables A2 to A8)

Table A2. Early MMN-related EEG findings in Sensor level Analysis: Summary of Post-hoc Analyses and Power Estimates. The left section reports results across Deviance (Large,

Intermediate, and Small) from one-way repeated-measures ANOVAs for each sensor-level region of interest (ROI), including F-values (F(2,26)), partial eta squared (η^2_p), Cohen's f, and estimated statistical power (1–β). The right section presents paired t-test comparisons (Large vs. Small and Large vs. Intermediate), with corresponding t-values (t(13), Cohen's d effect sizes, and power estimates. Effect sizes and power were calculated assuming n = 14 participants (df = 13).

	ANOVA				paired t-test comparisons			
ROI	**F**	**η^2_p**	**Cohen's f (ANOVA)**	**Power (1-β) ANOVA**	**Comparison**	**t**	**Cohen's d (t-test)**	**Power (1-β) t-test**
Frontal Left	9.00	0.41	0.83	0.99	Large vs Small	3.43	0.92	0.89
					Large vs Intermediate	3.54	0.95	0.90
Frontal Midline	8.34	0.39	0.80	0.99	Large vs Small	3.40	0.91	0.88
					Large vs Intermediate	2.74	0.73	0.71
Frontal Right	7.53	0.37	0.76	0.99	Large vs Small	3.69	0.99	0.93
					Large vs Intermediate	2.77	0.74	0.73
Central Midline	10.08	0.44	0.88	0.99	Large vs Small	3.83	1.02	0.94
					Large vs Intermediate	3.13	0.84	0.82

Table A3. Late MMN/N2-related EEG findings in Sensor level Analysis: Summary of Post-hoc Analyses and Power Estimates. The left section reports results across Deviance (Large, Intermediate, and Small) from one-way repeated-measures ANOVAs for each sensor-level region of interest (ROI), including F-values (F(2,26)), partial eta squared (η^2_p), Cohen's f, and estimated statistical power (1–β). The right section presents paired t-test comparisons (Large vs. Small and Large vs. Intermediate), with corresponding t-values (t(13), Cohen's d effect sizes, and power estimates. Effect sizes and power were calculated assuming n = 14 participants (df = 13).

	ANOVA				paired t-test comparisons			
ROI	**F**	**η^2_p**	**Cohen's f (ANOVA)**	**Power (1-β) ANOVA**	**Comparison**	**t**	**Cohen's d (t-test)**	**Power (1-β) t-test**
Frontal Midline	4.04	0.24	0.56	0.98	Large vs Small	2.25	0.60	0.55
					Large vs Intermediate	2.74	0.73	0.72
Central Midline	4.55	0.26	0.59	0.99	Large vs Small	3.14	0.84	0.83
					Large vs Intermediate	2.17	0.58	0.51

Table A4. Early MMNm-related MEG findings in Sensor level Analysis: Summary of Post Hoc Analyses and Power Estimates. The left section reports results across Deviance (Large, Intermediate, and Small) from one-way repeated-measures ANOVAs for each sensor-level region of interest (ROI), including F-values (F(2,26)), partial eta squared (η^2_p), Cohen's f, and estimated statistical power (1–β). The right section presents paired t-test comparisons (Large vs. Small and Large vs. Intermediate), with corresponding t-values (t(13), Cohen's d effect sizes, and power estimates. Effect sizes and power were calculated assuming n = 14 participants (df = 13).

	ANOVA				paired t-test comparisons			
ROI	**F**	**η^2_p**	**Cohen's f (ANOVA)**	**Power (1-β) ANOVA**	**Comparison**	**t**	**Cohen's d (t-test)**	**Power (1-β) t-test**
Central Left	12.71	0.49	0.99	0.99	Large vs Small	4.19	1.12	0.97
					Large vs Intermediate	3.32	0.89	0.88
Central Right	2.55	0.16	0.44	0.84	Large vs Small	4.09	1.09	0.97
					Large vs Intermediate	3.29	0.88	0.85
Parietal Left	17.10	0.57	1.15	0.99	Large vs Small	4.62	1.23	0.99
					Large vs Intermediate	4.29	1.15	0.97
Parietal Right	23.17	0.64	1.34	0.99	Large vs Small	5.59	1.49	0.99
					Large vs Intermediate	4.78	1.28	0.99

Table A5. Late MMNm/N2m-related MEG findings in Sensor level Analysis: Summary of Post Hoc Analyses and Power Estimates. The left section reports results across Deviance (Large, Intermediate, and Small) from one-way repeated-measures ANOVAs for each sensor-level region of interest (ROI), including F-values (F(2,26)), partial eta squared (η^2_p), Cohen's f, and estimated statistical power (1–β). The right section presents paired t-test comparisons (Large vs. Small and Large vs. Intermediate), with corresponding t-values (t(13), Cohen's d effect sizes, and power estimates. Effect sizes and power were calculated assuming n = 14 participants (df = 13).

	ANOVA				paired t-test comparisons			
ROI	**F**	**η^2_p**	**Cohen's f (ANOVA)**	**Power (1-β) ANOVA**	**Comparison**	**t**	**Cohen's d (t-test)**	**Power (1-β) t-test**
Central Left	5.55	0.30	0.65	0.99	Large vs Small	3.26	0.87	0.85
					Large vs Intermediate	2.33	0.62	0.58

	ANOVA				paired t-test comparisons			
Parietal Left	11.97	0.48	0.96	> 0.99	Large vs Small	3.38	0.90	0.87
					Large vs Intermediate	3.73	1.00	0.93
Parietal Right	3.41	0.21	0.51	0.96	Large vs Small	2.17	0.58	0.52
					Large vs Intermediate	1.56	0.42	0.30

Table A6. Early MMN-related EEG findings in Source level Analysis: Summary of Post Hoc Analyses and Power Estimates. The left section reports results across Deviance (Large, Intermediate, and Small) from one-way repeated-measures ANOVAs for each source-level region of interest (ROI), including F-values (F(2,26)), partial eta squared (η^2_p), Cohen's f, and estimated statistical power (1–β). The right section presents paired t-test comparisons (Large vs. Small and Large vs. Intermediate), with corresponding t-values (t(13), Cohen's d effect sizes, and power estimates. Effect sizes and power were calculated assuming n = 14 participants (df = 13).

	ANOVA				paired t-test comparisons			
ROI	**F**	**η^2_p**	**Cohen's f (ANOVA)**	**Power (1-β) ANOVA**	**Comparison**	**t**	**Cohen's d (t-test)**	**Power (1-β) t-test**
Left HG_1	11.47	0.47	0.94	> 0.99	Large vs Small	3.45	0.92	0.89
					Large vs Intermediate	3.52	0.94	0.90
Left HG_2	12.10	0.48	0.96	> 0.99	Large vs Small	3.60	0.96	0.91
					Large vs Intermediate	3.73	1.00	0.93
Right HG	11.69	0.47	0.95	> 0.99	Large vs Small	3.26	0.87	0.86
					Large vs Intermediate	4.00	1.07	0.96
Left SMG	9.07	0.41	0.84	> 0.99	Large vs Small	3.43	0.92	0.89
					Large vs Intermediate	2.73	0.73	0.71
Right SMG	7.21	0.36	0.74	> 0.99	Large vs Small	2.83	0.76	0.75
					Large vs Intermediate	2.65	0.71	0.69
Left STS1_1	7.44	0.36	0.76	> 0.99	Large vs Small	2.78	0.74	0.73
					Large vs Intermediate	2.91	0.78	0.77
Left STS1_2	7.86	0.38	0.78	> 0.99	Large vs Small	2.89	0.77	0.76
					Large vs Intermediate	3.13	0.84	0.83
Left STG	6.73	0.34	0.72	> 0.99	Large vs	2.74	0.73	0.72

	ANOVA				paired t-test comparisons			
					Small			
					Large vs Intermediate	2.59	0.69	0.67
Right STG_1	8.02	0.38	0.79	> 0.99	Large vs Small	2.81	0.75	0.74
					Large vs Intermediate	3.44	0.92	0.88
Right STG_2	6.78	0.34	0.72	> 0.99	Large vs Small	2.38	0.64	0.60
					Large vs Intermediate	3.55	0.95	0.91
Left Frontal Operculum	7.16	0.36	0.74	> 0.99	Large vs Small	2.54	0.68	0.66
					Large vs Intermediate	3.22	0.86	0.84
Right Frontal Operculum	4.33	0.25	0.58	> 0.99	Large vs Small	2.41	0.64	0.60
					Large vs Intermediate	2.65	0.71	0.69
Left IFG oper_2	5.36	0.29	0.64	> 0.99	Large vs Small	2.52	0.67	0.64
					Large vs Intermediate	3.16	0.84	0.83
Left Insula	9.09	0.41	0.84	> 0.99	Large vs Small	3.12	0.83	0.83
					Large vs Intermediate	3.13	0.84	0.83

Table A7. Early MMNm-related MEG findings in Source level Analysis: Summary of Post Hoc Analyses and Power Estimates. The left section reports results across Deviance (Large, Intermediate, and Small) from one-way repeated-measures ANOVAs for each source-level region of interest (ROI), including F-values (F(2,26)), partial eta squared (η^2_p), Cohen's f, and estimated statistical power (1–β). The right section presents paired t-test comparisons (Large vs. Small and Large vs. Intermediate), with corresponding t-values (t(13), Cohen's d effect sizes, and power estimates. Effect sizes and power were calculated assuming n = 14 participants (df = 13).

	ANOVA				paired t-test comparisons			
ROI	**F**	**η^2_p**	**Cohen's f (ANOVA)**	**Power (1-β) ANOVA**	**Comparison**	**t**	**Cohen's d (t-test)**	**Power (1-β) t-test**
Left HG_1	10.42	0.44	0.90	0.99	Large vs Small	3.32	0.89	0.86
					Large vs Intermediate	3.25	0.87	0.86
Left HG_2	13.06	0.50	1.00	0.99	Large vs Small	3.74	1.00	0.93
					Large vs Intermediate	3.62	0.97	0.91
Right HG	14.74	0.53	1.06	0.99	Large vs Small	3.82	1.02	0.94

	ANOVA				paired t-test comparisons			
					Large vs Intermediate	4.08	1.09	0.97
Right SMG	6.50	0.33	0.71	0.99	Large vs Small	3.24	0.87	0.85
					Large vs Intermediate	2.28	0.61	0.56
Left STG	8.02	0.38	0.79	0.99	Large vs Small	2.76	0.74	0.73
					Large vs Intermediate	3.57	0.95	0.91
Right STG_2	5.44	0.30	0.65	0.99	Large vs Small	2.83	0.76	0.75
					Large vs Intermediate	3.30	0.88	0.85
Left FrOper	12.13	0.48	0.97	0.99	Large vs Small	3.68	0.98	0.93
					Large vs Intermediate	3.44	0.92	0.89
Right FrOper	14.51	0.53	1.06	0.99	Large vs Small	3.84	1.03	0.95
					Large vs Intermediate	4.04	1.08	0.96
Left IFG oper_1	9.78	0.43	0.87	0.99	Large vs Small	2.99	0.80	0.78
					Large vs Intermediate	3.38	0.90	0.88
Left IFG oper_2	11.37	0.47	0.94	0.99	Large vs Small	3.34	0.89	0.87
					Large vs Intermediate	4.52	1.21	0.99
Left Insula	16.04	0.55	1.11	0.99	Large vs Small	4.20	1.12	0.97
					Large vs Intermediate	4.23	1.13	0.97

Table A8. Late MMNm/N2m-related MEG findings in Source level Analysis: Summary of Post Hoc Analyses and Power Estimates. The left section reports results across Deviance (Large, Intermediate, and Small) from one-way repeated-measures ANOVAs for each source-level region of interest (ROI), including F-values (F(2,26)), partial eta squared (η^2_p), Cohen's f, and estimated statistical power (1–β). The right section presents paired t-test comparisons (Large vs. Small and Large vs. Intermediate), with corresponding t-values (t(13), Cohen's d effect sizes, and power estimates. Effect sizes and power were calculated assuming n = 14 participants (df = 13).

	ANOVA				paired t-test comparisons			
ROI	**F**	**η^2_p**	**Cohen's f (ANOVA)**	**Power (1-β) ANOVA**	**Comparison**	**t**	**Cohen's d (t-test)**	**Power (1-β) t-test**
Left HG_1	4.56	0.26	0.59	0.99	Large vs Small 0.96	0.96	0.26	0.14
					Large vs	2.87	0.77	0.75

	ANOVA				paired t-test comparisons			
					Intermediate			
Right STG_1	4.33	0.25	0.58	0.99	Large vs Small	3.05	0.82	0.81
					Large vs Intermediate	1.95	0.52	0.44

1432